INPP4B promotes leukemia by restricting leukemic stem cell differentiation through regulation of lysosomal functions

Authors:

John F. Woolley[1,2,‡*], Keyue Chen[1], Gizem E. Genc[3], Daniel K.C. Lee[1], Irakli Dzneladze[2], Ruijuan He[2], Martino M. Gabra[1], Golam T. Saffi[1], Meong Hi Son[1,2,§], Erwin M. Schoof[2], Stephanie Z. Xie[2], Max Kotlyar[5], Ayesha Rashid[2], Jean Vacher[4], Igor Jurisica[5,6,7,8], John E. Dick[2,9,10], Roberto J. Botelho[3], Mark D. Minden[2,7], and Leonardo Salmena[1,2,11*]

Affiliations:

[1] Department of Pharmacology & Toxicology, University of Toronto, Toronto, Ontario M5S 1A8, Canada

[2] Princess Margaret Cancer Centre, University Health Network, Toronto, Ontario M5G 1L7, Canada

[3] Department of Chemistry and Biology, Ryerson University, Toronto, Ontario M5B 2K3, Canada

[4] Institut de Recherches Cliniques de Montréal (IRCM), Département de Médecine, Université de Montréal, Montréal, Québec H2W 1R7, Canada

[5] Osteoarthritis Research Program, Division of Orthopedic Surgery, Schroeder Arthritis Institute, University Health Network; Data Science Discovery Centre for Chronic Diseases, Krembil Research Institute, University Health Network, Toronto, Ontario M5T 0S8, Canada.

[6] Department of Computer Science, University of Toronto, Toronto, Ontario M5T 3A1, Canada

[7] Departments of Medical Biophysics, University of Toronto, Toronto, Ontario M5G 1L7, Canada

[8] Institute of Neuroimmunology, Slovak Academy of Sciences, Bratislava, Slovakia

[9] Department of Molecular Genetics, University of Toronto, Toronto, Ontario M5S 1A8, Canada

[10] Ontario Institute for Cancer Research, Toronto, Ontario M5G 0A3, Canada

[11] Lead Contact

Author list footnotes:

[‡]Present address: Department of Pharmacology & Therapeutics, Institute of Systems, Molecular and Integrative Biology, University of Liverpool, UK.

[§]Present address: Department of Pediatrics, Samsung Medical Center, Sungkyunkwan University School of Medicine, Seoul, Korea

*Correspondence: john.woolley@liverpool.ac.uk (J.F.W); leonardo.salmena@utoronto.ca (L.S.)

Summary

Despite an increased understanding of leukemogenesis, specific mechanisms that underlie 'stemness' in leukemia remain largely undefined. Here, we report a novel pathway which regulates leukemic differentiation through control of lysosomal biology. We show that disruption of INPP4B results in dysregulated lysosomal gene networks, reduced lysosomal numbers and proteolytic capacity in leukemia. *Inpp4b*-deficient HSCs and LSCs are functionally compromised. *Inpp4b*-deficient leukemia models develop more differentiated leukemias with reduced disease initiating potential, and improved overall survival compared to *Inpp4b*-expressing leukemias. Together, our data is consistent with a model where INPP4B restricts differentiation of LSCs through regulation of lysosomal function. These data provide a mechanism to explain the association of INPP4B with aggressive AML and highlight avenues for LSC-specific leukemia therapies.

Keywords

INPP4B, AML, LSC, lysosome, differentiation

Introduction

Acute myeloid leukemia (AML) is an aggressive malignancy of the bone marrow characterized by dysregulated proliferation of immature myeloid cells and dismal survival rates (Estey and Döhner, 2006; Klepin et al., 2014; Löwenberg et al., 1999). Most AML patients who receive intensive chemotherapy achieve a significant clinical response, however a majority will relapse within 5 years and succumb to their disease (Grimwade et al., 2010; Walter et al., 2015). Thus, AML remains a largely incurable cancer, due to disease relapse and chemoresistance.

AML has been shown to exist as a cellular hierarchy, with leukemic stem cells (LSC) at the pinnacle which possess 'stemness' attributes including a capacity for self-renewal, differentiation, long-term clonal propagation and quiescence, which all serve to continuously sustain a bulk of malignant undifferentiated myeloid 'blast' cells that define AML (Dick, 2008). It has been demonstrated that AML patients with greater LSC content and more stem-like disease have worse clinical outcomes (Eppert et al., 2011; Ng et al., 2016; van Rhenen et al., 2005; Shlush et al., 2017). Thus, in the absence of LSC-eradicating therapies it is not surprising that relapse occurs in the majority of AML patients. Despite an increased understanding of AML and leukemogenesis over the past decades, specific molecular machinery that underlie 'stemness' in AML remains largely undefined.

The lysosome is a major platform for many cellular signaling pathways including cell growth, division, differentiation (Inpanathan and Botelho, 2019; Lawrence and Zoncu, 2019); however, distinct lysosomal activities in stem cells are still emerging. Functional lysosomes in neuronal stem cells are needed to mitigate protein-aggregate accumulation, a consequence which would otherwise increase aging, reduce stem functions and lead to differentiation of these cells (Leeman et al., 2018). Emerging studies in hematopoietic stem cells (HSC) suggest that lysosomes are asymmetrically inherited and thus predictive of future daughter cell fates (Loeffler et al., 2019); pharmacological inhibition of the lysosomal v-ATPase can positively impacted mouse HSC engraftment (Liang et al., 2020), lysosomes have been shown to coordinate the cell cycle and metabolic machinery of LT-HSC through their ability

to sense and respond to diverse signaling cues (García-Prat et al., 2021). In leukemia, increased lysosomal mass and biogenesis in leukemic progenitor cells selectively sensitizes AML cells to lysosomal inhibitors or disruptors (Sukhai et al. 2013; Bernard et al. 2015). Nevertheless, roles for lysosome in LSC and leukemic differentiation remain largely unknown.

We previously reported that *Inositol Polyphosphate-4-Phosphatase Type II (INPP4B)*, a lipid phosphatase that hydrolyzes phosphatidylinositol-3,4-bisphosphate [PtdIns(3,4)P_2] to generate phosphatidylinositol-3-monophosphate [PtdIns(3)P] demonstrates elevated expression levels in the leukemic blasts of approximately one quarter of all AML patients (Dzneladze et al., 2015). Studies from our group and others in AML (Dzneladze et al., 2015; Jin et al., 2018; Recher, 2015; Rijal et al., 2015; Wang et al., 2016; Zhang et al., 2017, 2019) and other malignancies (Chi et al., 2015; Gasser et al., 2014; Guo et al., 2016) demonstrate that INPP4B possesses tumour promoting and oncogenic functions. These findings prompted us to investigate specific roles of INPP4B in hematopoiesis and leukemogenesis. Herein we report novel functions for INPP4B in hematopoietic stemness and a role for INPP4B in restricting the differentiation of LSC through the regulation of lysosome biology and function.

Results

Hematopoietic stem and progenitor cell populations express elevated levels of *INPP4B*

To investigate a role for INPP4B in hematopoiesis, we first interrogated expression datasets derived from purified human (Jung et al., 2015; Laurenti et al., 2013, 2015; Lechman et al., 2016; Notta et al., 2016; Novershtern et al., 2011; Rapin et al., 2014) and mouse (Lara-Astiaso et al., 2014; Pietras et al., 2015) hematopoietic stem and progenitor cell (HSPC) populations datasets. We observed that the expression of *INPP4B* is consistently highest in HSPC populations with the greatest pluripotency and self-renewal potential [eg. long-term (LT)-HSCs, short-term (ST)-HSCs and multipotent progenitor cells (MPPs)]; progressively lower levels of expression were observed in committed progenitors and

terminally differentiated myeloid lineage cells including granulocytes and monocytes (**Fig. 1A and Supplementary 1A**). Similarly, in murine datasets, *Inpp4b* expression was highest in LT-HSCs and bulk HSCs, with lower levels found in lineage restricted HSPCs and terminally differentiated populations (**Fig. 1B and Supplementary 1B**). These data indicate that *INPP4B* expression is associated with HSPC pluripotency, pointing to a putative role for INPP4B in HSC maintenance(**Fig. 1C**).

Inpp4b deficiency leads to alterations in hematopoietic progenitor populations

To study *Inpp4b* function in HSPCs, we employed a constitutive *Inpp4b*-knockout mouse model (*Inpp4b*$^{-/-}$) generated by Vacher and colleagues (Ferron et al., 2011). *Inpp4b*$^{-/-}$ and *Inpp4b*$^{+/-}$ mice are viable and born at the expected Mendelian frequencies. We did not observe the occurrence of any cancers or premature lethality in *Inpp4b*$^{-/-}$ or *Inpp4b*$^{+/-}$ mice up to and beyond 2 years of age consistent with other published *Inpp4b* mouse models (Kofuji et al., 2015; Li Chew et al., 2015). In this study we focused our analysis of the knockout animals to the hematological system. Gross hematological phenotypes in 6-10 weeks old *Inpp4b*$^{-/-}$ or *Inpp4b*$^{+/+}$ mice demonstrated no measurable differences in total bone marrow cellularity, circulating white blood cell counts, lymphocytes, monocytes, neutrophils, red blood cells and platelet numbers in peripheral blood (**Fig. Supplementary 1C, 1D**).

In contrast, flow cytometric analysis of progenitor populations from adult *Inpp4b*$^{+/+}$ and *Inpp4b*$^{-/-}$ mice (>6 weeks of age) revealed a marked reduction in the number of LSK (Lin^{-}Sca-1^{+}c-Kit^{+}), short-term HSCs (ST-HSC; CD34^{+}CD150^{+}CD48^{-}LSK) and long-term HSC (LT-HSC; CD34^{-}CD150^{+}CD48^{-} LSK or EPCR^{+}LSK) (**Fig. 1D,E; Fig. Supplementary 1E,F**), and a suggestive reduction in multipotent progenitors (MPP) (**Fig. 1E**) in *Inpp4b*$^{-/-}$ as compared to *Inpp4b*$^{+/+}$ mice. Granulocyte monocyte progenitors (GMP) were significantly reduced, and megakaryocyte erythrocyte progenitors (MEP) were significantly increased in *Inpp4b*$^{-/-}$ bone marrow compared to *Inpp4b*$^{+/+}$ bone marrow. No differences

were observed in common myeloid progenitor (CMP) and lymphomyeloid-primed progenitor (LMPP) fractions **(Fig 1F)**. Together, these findings suggest a role for *Inpp4b* expression in the homeostasis of HSPC populations.

Hematopoietic stem cells have reduced function in *Inpp4b* knock-out mice

To measure functional consequences of *Inpp4b*-deficiency on defining hallmarks of HSC including self-renewal, differentiation, and long-term clonal propagation we tested *wild type* and *Inpp4b*-deficient HSC functionality both *in vitro* and *in vivo*. First, we evaluated the *in vitro* colony forming and self-renewal potential of bone marrow cells from *Inpp4b*$^{+/+}$ and *Inpp4b*$^{-/-}$ mice using colony-forming cell (CFC) assays with serial replating every seven days for a total of 4 weeks (**Fig. 2A**). Seven days after the initial plating, we observed no difference in the number of total colonies between *Inpp4b*$^{+/+}$and *Inpp4b*$^{-/-}$ colony numbers. However, upon subsequent re-plating of colonies, total colony numbers from *Inpp4b*$^{-/-}$ bone marrow were significantly reduced (day 14: 126 ± 8.4 *vs* 94 ± 8.2), with further reduction evident after the third plating (day 21: 105 ± 15.0 *vs* 14 ± 3.9) indicating a premature collapse of colony forming capacity of *Inpp4b*$^{-/-}$ bone marrow cells. The reduction in total colony numbers at day 14 between *Inpp4b*$^{+/+}$ and *Inpp4b*$^{-/-}$ was predominantly a result of fewer CFU-M colonies in *Inpp4b*$^{-/-}$ compared to other lineages (**Fig. Supplementary 2A**) suggesting that *Inpp4b*-deficiency leads to a defect in the differentiation of myeloid-committed precursors, particularly of the monocyte lineage. By day 21, there was premature collapse of all lineages in *Inpp4b*$^{-/-}$ progenitors (**Fig. 2A, Fig. Supplementary 2A)**.

To investigate whether *Inpp4b*-deficiency impacts the repopulation potential of HSCs *in vivo*, we challenged *Inpp4b*$^{+/+}$ and *Inpp4b*$^{-/-}$ mice with a myeloablation regimen of weekly i.p. injections of 5'-fluorouracil (5'-FU). Survival analysis demonstrated that *Inpp4b*$^{-/-}$ mice had a significantly reduced overall survival (median survival 24 days) compared to wild-type littermates (P = 0.008; median

survival 28 days) upon serial myeloablation (**Fig. 2B**). To estimate the relative quiescence of HSCs upon 5'-FU treatment *in vivo*, we performed Ki67 staining of sorted HSPCs ($Lin^{-}Sca\text{-}1^{+}Kit^{+}$) 48 hours after a single acute treatment of 5'-FU. We observed that *Inpp4b*$^{-/-}$ HSPCs had a significant increase in cycling cells as compared to *Inpp4b*$^{+/+}$ HSPCs (**Fig. 2C**). Together, these data suggest that the induction of replicative-stress by serial myeloablation in *Inpp4b*$^{-/-}$ mice leads to an aberrant escape-from-quiescence of hematopoietic progenitor associated with premature lethality.

Next, to evaluate the contribution of *Inpp4b* to the long-term repopulation capacity of HSPCs we carried out a serial competitive transplant assays with *Inpp4b*$^{+/+}$, *Inpp4b*$^{+/-}$ and *Inpp4b*$^{-/-}$ bone marrow where LT-HSC output was determined as the relative contribution of CD45.1 (competitor HSPCs) and CD45.2 (test HSPCs) to the myeloid lineage over 20 weeks post-transplant, in 3 consecutive *in vivo* repopulation experiments (**Fig. 2D, E, Fig. Supplementary 2B**). Notably, at the end of the primary competitive transplant at week 20 we observed that unlike *Inpp4b*$^{+/+}$ HSPCs which contribute half (50%) of total myeloid cells, *Inpp4b*$^{-/-}$ (78.5%) and *Inpp4b*$^{+/-}$ (70.0%) HSPCs outcompeted *Inpp4b*$^{+/+}$ HSPCs. However, at the end of the experiment at 64 weeks, we observed that both *Inpp4b*$^{+/-}$ and *Inpp4b*$^{-/-}$ bone marrow cells demonstrated a near-complete loss of contribution to the myeloid compartment compared to *Inpp4b*$^{+/+}$ bone marrow, demonstrating that long-term hematopoietic reconstitution is significantly compromised with *Inpp4b*-deficiency. The increased contribution of the *Inpp4b*$^{-/-}$ and *Inpp4b*$^{+/-}$cells at the first time point may be due to the increased rate of proliferation and failure of these cells to return to rest as observed in **Fig 2C**. At the end of the second transplant (44 weeks), *Inpp4b*$^{+/+}$ HSPCs continue to contribute approximately half (44%) of the total donor derived myeloid cells. However, in contrast to the earlier time point *Inpp4b*$^{-/-}$ HSPCs demonstrate a reduced reconstitution capacity at 27% and *Inpp4b*$^{+/-}$ HSPCs continue to outcompete *Inpp4b*$^{+/+}$ at 73% of total myeloid cells. Taken together these data indicate that *Inpp4b*-deficient HSCs have a reduced capacity for long-term hematopoietic repopulation as a result of elevated sensitivity to replicative stress.

INPP4B expression is associated with leukemic stemness gene networks

Given the role we have demonstrated for INPP4B in hematopoiesis combined with our previous data demonstrating a role for INPP4B in AML prognosis (Dzneladze et al., 2015; Rijal et al., 2015) we reasoned that INPP4B may also play a role in leukemogenesis and LSC biology. Interestingly, *INPP4B* is one of forty-four genes enriched in HSCs and LSCs gene profiles(Eppert et al., 2011). Furthermore, we interrogated *INPP4B* expression in gene expression profiles from a total of 227 AML patient-derived cells sorted based on the expression of combinations of CD34 and CD38 surface markers (Ng et al., 2016). We observed the highest levels of *INPP4B* transcript in $CD34^{+}CD38^{-}$ > $CD34^{+}CD38^{+}$ > $CD34^{-}CD38^{-}$ > $CD34^{-}CD38^{+}$ (**Fig. 3A**), where $CD34^{+}CD38^{-}$ populations are considered to be enriched for LSC content compared to other AML subsets. In keeping with the notion that LSC and their capacity for disease reconstitution is not defined solely on the basis of the $CD34^{+}CD38^{-}$ phenotype, we also interrogated datasets from LSC populations defined functionally through bone marrow transplant experiments (Eppert et al., 2011; Ng et al., 2016). We observed that gene expression profiles from 278 CD34/CD38 sorted populations derived from 78 AML patients (Ng et al., 2016) had significantly elevated levels of *INPP4B* expression and the $INPP4B^{high}$ samples in functionally defined LSC had an odds ratio of ~6 for association with functionally defined LSC^{+} populations (Chi-square *P*-value < 0.0001) (**Fig. 3B**). Furthermore, using gene-set enrichment analysis (GSEA) we investigated the association of high *INPP4B* expression to the LSC17 signature genes (Ng et al., 2016) in six public AML patient databases (Balgobind et al., 2011; Cancer Genome Atlas Research Network et al., 2013; Klein et al., 2009; Metzeler et al., 2008; Verhaak et al., 2009). We observed that the LSC-17 signature was significantly enriched in patient samples with high *INPP4B* expression in all AML patient databases tested (**Fig. 3C & Supplementary Fig. 3**). Altogether, our analyses of *INPP4B* gene expression in AML

subsets and functionally defined LSC populations are the first data pointing to an association between *INPP4B* and leukemic stemness.

Inpp4b-deficiency leads to increased disease latency and a more differentiated leukemia

To investigate a direct role for *Inpp4b* in leukemogenesis and LSC function *in vivo*, we generated a model of *Inpp4b*-deficient leukemia by transducing *Inpp4b*$^{-/-}$ LSK cells and control *Inpp4b*$^{+/+}$ LSK cells with MSCV-*MLL-AF9-Venus* retrovirus. Venus^{+}*Inpp4b*$^{-/-}$ and Venus^{+}*Inpp4b*$^{+/+}$ LSK cells were transplanted by tail vein injection into sub-lethally irradiated syngeneic host C57BL/6 mice to promote the development of primary leukemias **(Supplementary Fig. 4A**). Notably, all host animals transplanted with *Inpp4b*$^{+/+}$ *MLL-AF9*-infected cells succumbed to leukemia associated disease, however ~40% of the host animals transplanted with *Inpp4b*$^{-/-}$*-MLL-AF9* leukemia cells survived beyond 300 days suggesting that *Inpp4b*$^{-/-}$-leukemias have decreased potential to kill the animals either due to overwhelming leukemia or failure of normal hematopoiesis (**Fig. 4A**). In support of this, secondary transplants of *MLL-AF9* leukemias **(Fig. 4B**) also demonstrated a significant increase in disease latency for the *Inpp4b*$^{-/-}$*-MLL-AF9* when compared to the *Inpp4b*$^{+/+}$*-MLL-AF9* (median survival of 76 *vs.* 41 days respectively; p=0.0246). Furthermore, limiting dilution cell transplantation assays (LDA) revealed that *Inpp4b*$^{-/-}$*-MLL-AF9* leukemias have a significant decrease (1/147 *vs* 1/300 P = 0.0331) in leukemic initiating cell (LIC) frequency (**Fig. 4C)**.

Leukemia forming cell (LFC) assays carried out with primary *Inpp4b*$^{+/+}$ and *Inpp4b*$^{-/-}$ *MLL-AF9* leukemic cells demonstrated that *Inpp4b*-deficiency leads to a significant decrease in total leukemic colonies formed (**Fig. 4D)**. Furthermore, *Inpp4b*-deficiency leads to a decrease in the percentage of type-I colonies (spherical with defined border, resembling primitive hematopoietic colony formation) countered by an increase in more differentiated type-II colonies (diffuse, lacking a defined border) (**Fig. 4D)** (Krivtsov et al., 2006; Somervaille and Cleary, 2006). Wright–Giemsa staining of leukemic smears

revealed a more differentiated blast cell phenotype in *Inpp4b*$^{-/-}$ *MLL-AF9* as determined by an elevated proportion of multi-lobed, horseshoe-shaped or diffuse nuclei (**Fig. 4E**). Only 16.9% of *Inpp4b*$^{+/+}$ *MLL-AF9* leukemia cells had a differentiated morphology, whereas 51.6% of *Inpp4b*$^{-/-}$*-MLL-AF9* leukemias had a differentiated phenotype. To support these observations, we simultaneously evaluated the expression of several cell-surface markers associated with myeloid leukemia differentiation by mass cytometry (**Supplementary Fig. 4B,C**). Among several cell-surface markers with significantly altered fluorescence intensities, increased expression of CD24, Gr-1 and CD117, and decreased Flt3 surface expression was observed in the *Inpp4b*$^{-/-}$ *MLL-AF9* leukemias (**Fig. 4F,G and Supplementary Fig. 4D**) in keeping with a more differentiated myeloid phenotype (Saadatpour et al., 2014). Taken together, these data indicate that *Inpp4b*-deficiency in an *MLL-AF9* leukemia model generates leukemias with decreased colony forming potential, altered morphology and cell surface marker expression which is consistent with the observed decrease in leukemogenic potential (Somervaille and Cleary, 2006)**.**

Identification of transcriptional networks perturbed by *Inpp4b* loss in leukemia cells

To identify the consequences of *Inpp4b* deficiency in leukemic transcriptional networks we performed RNA sequencing (RNA-seq) on freshly isolated bone marrow from *Inpp4b*$^{+/+}$ and *Inpp4b*$^{-/-}$ *MLL-AF9* leukemias. RNA-seq revealed a total of 5462 differentially expressed genes between *Inpp4b*$^{+/+}$ and *Inpp4b*$^{-/-}$ *MLL-AF9* leukemias (2434 downregulated, 3028 upregulated; FDR < 0.05; **Supplementary Fig. 5A,B**, **Supplementary Table 1).**

To identify biological processes most significantly influenced by *Inpp4b* deficiency, we performed gene ontology (GO) and Gene Set Enrichment Analysis (GSEA) on the differentially expressed gene list (**Fig. 5A,B; Supplementary Table 2**). Both analyses revealed enrichment of lysosomal gene sets (eg. 64 out of 124 genes in the Kyoto Encyclopedia of Genes and Genomes (KEGG) lysosomal gene signature; corrected *P*-value = 3.62×10^{-06}). Gene profiling demonstrated that a

disproportionately large number of KEGG lysosomal gene transcripts were downregulated in *Inpp4b*$^{-/-}$ *MLL-AF9* gene profiles compared to *Inpp4b*$^{+/+}$ controls (**Fig. 5C**). Using data generated by STRING-db, we observed that the KEGG lysosome signature gene set could be subdivided into three protein interaction networks: trans-golgi network trafficking proteins, vacuolar ATPases and lysosome-active proteins and transporters. Although we observed loss of gene expression in all three subdivisions, the most notable losses were strongly associated with lysosome-active proteins and transporters including several cathepsins (*Ctss, Ctsc and Ctsf*), lysosomal transporters (*Slc11a1*) and other proteases (*Lgmn, Psap, Lipa*) (**Fig. 5C,D**). To further the association between *Inpp4b* expression with lysosomal transcripts (**Fig. 5E)**, we performed GSEA using an independent set of transcription factor EB (TFEB)-regulated lysosomal genes from the Coordinated Lysosomal Expression and Regulation (CLEAR) network (**Fig. 5F)** with similar results (Sardiello et al., 2009). Together these results point to a role for Inpp4b in regulating lysosomal biology through regulation of lysosomal gene expression.

To further support the notion that *Inpp4b* deficiency was associated with a phenotypically differentiated leukemia we investigated the presence of changes in genes and networks associated with leukemic stemness or myeloid differentiation. Using GSEA we observed that there were significant changes in the LSC17 gene signature (**Fig 5G**), a myeloid cell development signature and an osteoclast differentiation signature (**Supplementary Fig 5C,D**) in *Inpp4b*-deficiency (Mootha et al., 2003; Ng et al., 2016; Subramanian et al., 2005). These findings indicate that *Inpp4b*-deficiency in *MLL-AF9* leukemia significantly alters gene transcription networks associated with lysosome biology, myeloid stemness and myeloid lineage differentiation.

INPP4B expression in human AML is associated with a lysosomal gene signature

Given our results linking *Inpp4b*-deficiency with disrupted lysosomal gene networks in murine leukemia, we investigated the presence of an orthologous association in human leukemia. For this we

interrogated the TCGA-LAML and Verhaak-AML patient datasets, two of the largest publicly available AML datasets using GSEA (Cancer Genome Atlas Research Network et al., 2013; Mootha et al., 2003; Subramanian et al., 2005; Verhaak et al., 2009). Using a previously established optimal cutoff of 75% for *INPP4B* high/low expression and patient outcome in AML datasets as determined by our subgroup identifier (SubID) tool (Dzneladze et al., 2015, 2018), we identified the top 20 most enriched KEGG-defined gene sets associated with *INPP4B* expression. Notably, the lysosome, and other lysosome-related gene sets including glycosaminoglycan degradation and other glycan degradation gene sets were ranked among the top significantly enriched gene sets in both TCGA (NES=1.74, NOM p = 0.02) and Verhaak (NES=1.90, NOM p = 0.02) datasets (**Fig 6A-D, Supplemental Fig 6A,B**). Similar associations with the KEGG lysosomal gene set were observed in additional AML patient datasets from studies by Valk (NES=1.92, NOM $p < 0.0001$) and Wouters (NES=1.56, NOM p = 0.02) (**Fig 6E,F; Supplemental Fig 6C,D**)(Valk et al., 2004; Wouters et al., 2009). Furthermore, among the 121 genes which comprise the lysosome gene set, 78 genes were classified as leading-edge genes (LEGs) in at least one of the TCGA, Verhaak, Valk and Wouters datasets, and a core set of 30 LEGs were present in all 4 datasets (**Fig 6G,H**). Together, the results of our analysis of public AML datasets support our results in murine leukemia models and show that the expression of *INPP4B* and core lysosomal genes are associated across various AML patient datasets.

INPP4B regulates lysosomal biology

To substantiate our transcriptional and correlative data, we investigated a direct role for INPP4B in lysosome biology by measuring the consequences of INPP4B overexpression or knockdown on lysosomal characteristics in cancer cell lines. For these studies we generated inducible *INPP4B*-U2OS osteosarcoma cells by inserting a donor vector sequence containing an inducible TRE3G-*INPP4B* and constitutive Tet-On 3G expression cassettes into the *AAVS1* safe harbor locus by CRISPR genome

editing (Mandegar et al., 2016). Lysosomal Associated Membrane Protein 1 (LAMP1), a type I membrane protein possessing a short cytosolic C-terminus harboring an endo-lysosomal targeting sequence, was used as a representative lysosomal marker (Bagshaw et al., 2005a, 2005b; Callahan et al., 2009). We evaluated cytoplasmic LAMP-1 puncta in the presence and absence of INPP4B induction using 100 ng/mL of doxycycline (**Fig 7A**). Upon induction of INPP4B, we observed a significant increase in the number of LAMP1 puncta (**Fig 7A)** and an increase in the total cellular intensity of LAMP1 staining (**Supplemental Fig 7A**). Conversely, siRNA-knockdown of INPP4B (**Fig 7B**) was associated with significantly decreased number of LAMP1 puncta (**Fig 7B**) and decreased intensity (**Supplemental Fig 7B**) compared to non-targeting siRNA (siNC; **Fig 7B**).

The cellular positioning of lysosomes also plays an important role in lysosomal function (Cabukusta and Neefjes, 2018; Korolchuk et al., 2011; Pu et al., 2016; Settembre et al., 2012). Thus, we measured the extent of lysosomal dispersion in *INPP4B* overexpressing and knockdown cells by demarcating the cytoplasm of cells into 4 shells beginning with a perinuclear shell (**Fig 7C**). We observed that INPP4B overexpression led to an increased number of LAMP1 puncta in all peripheral shells, with no change in the inner perinuclear shell (**Fig 7D**). Conversely, LAMP1 dispersion upon INPP4B knockdown with INPP4B-siRNA did not significantly change lysosomal distribution compared to control cells (**Fig 7E**). To measure a role for INPP4B in regulating the proteolytic capacity of lysosomes, we incubated cells with (DQ)-BSA-Green, a quenched dye which generates bright fluorescence upon proteolysis within lysosomes. In these experiments, cells were allowed to simultaneously endocytose DQ-BSA-Green and fluorescent-tagged Dextran-Red. The latter is always fluorescent and can be normalized against DQ-BSA to control for any differences in the endocytosis rate of DQ-BSA, which in turn would affect DQ-BSA fluorescence. We observed that *INPP4B* overexpression resulted in activation of significantly greater levels of DQ-BSA fluorescence compared to controls (**Fig 7F**). Conversely, decreased DQ-BSA fluorescence was measured in INPP4B-

knockdown cells when compared to controls (**Fig 7G**). Together, these results are the first demonstration of a role for INPP4B in regulating lysosomal content, dispersion and proteolytic function.

To provide evidence for a direct role for INPP4B on lysosomes, we examined whether INPP4B can localize to lysosomes. For these experiments, first we overexpressed mCherry-INPP4B in U2OS cells and measured colocalization to lysosomes labelled with Lucifer Yellow. We observed a significant increase in INPP4B-mCherry localization to lysosomes when compared to empty-mCherry vector **(Supplemental Fig 7C-D**). Colocalization of INPP4B-mCherry with Lucifer Yellow stained lysosomes was measured to be stable for at least 20 min **(Supplemental Fig 7E,F**). Furthermore, immunoblotting of lysosomal immunoprecipitations confirmed the interaction of overexpressed INPP4B with lysosomes **(Supplemental Fig 7G).**

INPP4B controls lysosomal function and response to lysosomal inhibition in leukemia cells

To investigate a role for INPP4B in lysosomal biology in leukemia cells, we generated OCI-AML2 cells with inducible-INPP4B as described above. These cells were incubated with DQ-BSA-Green, and fluorescence was monitored by flow cytometry hourly, for 6 hours. INPP4B overexpressing cells proteolytically activated significantly greater levels (ANOVA *P*-value > 0.0001 P > 0.0001**(Supplemental Fig 8A**)) of DQ-BSA-Green fluorescence compared to controls at each time point (**Fig. 8A**). Similarly, experiments conducted in *Inpp4b*$^{+/+}$ and *Inpp4b*$^{-/-}$ *MLL-AF9* leukemias for up to 8 hours showed that *Inpp4b*$^{-/-}$ leukemia cells had significantly lower levels of DQ-BSA-Green fluorescence throughout the time-course after incubation (ANOVA *P*-value > 0.0001; **(Fig. 8B, Supplemental Fig 8B**)). Cellular uptake of fluorescence-labelled Dextran was no different in INPP4B overexpressing or control OCI-AML2 cells, nor *Inpp4b*$^{+/+}$ and *Inpp4b*$^{-/-}$ *MLL-AF9* leukemia cells, indicating that endocytic uptake wsa similar and thus not responsible for the differential levels of DQ-BSA-Green activation (**Supplemental Fig 8A-B**).

Given the observations that INPP4B expression restricts leukemic differentiation and regulates lysosome function, we reasoned that lysosomes may be involved in maintaining leukemic cells in a more stem-like state. To test this hypothesis, we treated *Inpp4b*$^{+/+}$ and *Inpp4b*$^{-/-}$ *MLL-AF9* leukemia cells with the lysosome inhibitor Lys05 followed by LFC assays (Amaravadi and Winkler, 2012; Cechakova et al., 2019; McAfee et al., 2012). We observed that Lys05 reduced colony forming potential of all *MLL-AF9* leukemia cells in a dose dependent manner. Lys05 treatment was significantly more consequential for the colony forming potential of *Inpp4b*$^{+/+}$ cells as compared to *Inpp4b*$^{-/-}$ cells (**Fig. 8C)**. Moreover, we observed that more primitive type-I colonies were decreased with increasing doses of Lys05, whereas the more differentiated type-II colonies were increased (**Fig. 8D)**. Together, these data show that normal lysosomal function is dependent on the presence of Inpp4b. Accordingly, the leukemic differentiating effects of lysosome inhibition with Lys05 is blunted in *Inpp4b*-deficient cells. These findings are in line with a model where INPP4B restricts leukemia differentiation through the control of lysosome function.

Discussion

Although previous studies have demonstrated that *INPP4B* overexpression in AML is an independent prognostic marker for poor disease outcome and a predictor of chemotherapy (Dzneladze et al., 2015; Recher, 2015; Rijal et al., 2015; Wang et al., 2016; Zhang et al., 2017), how INPP4B drives AML is poorly understood. Our studies present several lines of evidence supporting a role for INPP4B in HSC and LSC pluripotency through the regulation of lysosome biology. By investigating the consequences of *Inpp4b*-deficiency in both hematopoiesis and leukemogenesis in *Inpp4b*-knockout mouse, combined with analysis of *INPP4B* expression in a number of human AML patient databases and cell models, we discovered that (1) *INPP4B* expression is enriched in primordial HSC and LSC; (2) *Inpp4b*-deficient leukemias have more differentiated phenotypes and exhibit increased disease latency; (3) Lysosome gene networks and function are regulated by INPP4B; (4) Disruption of lysosome

functions by either INPP4B depletion or direct pharmacological inhibition leads to leukemic differentiation. Overall, by delineating INPP4B functions in AML, we have unveiled critical pathways that may underlie 'stemness' in leukemia.

INPP4B expression was elevated in the most pluripotent cells of hematopoietic lineages and leukemia populations and was decreased in more differentiated populations. These data pointed to a role for INPP4B in restricting differentiation, which was confirmed in *Inpp4b*-deficient mice where long term repopulation of HSCs was compromised. Notably, we also observed a marked increase in cycling of *Inpp4b*-deficient HSCs upon myeloablation and or bone marrow reconstitution prior to exhaustion, suggesting that Inpp4b may regulate the ability of HSC to achieve quiescence after replicative stresses. *Inpp4b* expression mirrors the pattern of expression of genes with known HSC function over the course of 20 weeks of xenotransplant (Laurenti et al., 2015), decreasing as bone-marrow resident HSCs escape quiescence (up to week 4) before returning to steady-state levels as the homeostasis returns (week 20). These findings are consistent with a model where Inpp4b-deficiency limits the ability of the HSC population to remain in quiescence, instead cells experience excessive proliferation and ultimately suffer from long-term HSC exhaustion.

Analogously, *Inpp4b*$^{-/-}$ leukemias generated using the *MLL-AF9* oncogenic fusion protein, have a more differentiated AML phenotype and reduced leukemia initiating potential, further supporting a role for Inpp4b in maintaining 'stemness'. Our findings linking INPP4B to leukemia stemness identifies it as a putative therapeutic target, with potential to compromise LSC self-renewal function and consequently drive differentiation. However, given that INPP4B inhibition is not currently achievable, we sought to investigate processes downstream of INPP4B signalling with pharmacological potential. RNA sequencing of *Inpp4b*$^{+/+}$ and *Inpp4b*$^{-/-}$ leukemia combined with gene network analyses revealed that the expression of a number of key lysosomal genes including proteases and membrane transporters are under the control of Inpp4b expression. This was mirrored in AML patient data, where lysosomal gene

networks were significantly associated with high INPP4B expression. Importantly, cell models of INPP4B loss and overexpression confirm that INPP4B regulates lysosome biology, including lysosomal quantity, cellular dispersion of lysosomes as well as proteolytic capacity.

Today, the lysosome is known to be a critical platform for cellular signaling that governs cell growth, division and differentiation through the integration of metabolic, nutrient and growth factor signals. Of particular importance for lysosomal functions is its intimate relationship mTORC1, the master regulator of energy and nutrient signaling (Saxton and Sabatini 2017). A direct substrate of mTORC1 is the transcription factor TFEB which regulates the transcription of a large network of lysosomal genes and thereby governs lysosomal biogenesis (Perera et al., 2019). Although INPP4B has not yet been directly linked to mTORC1 activation, its major phosphoinositide substrate PtdIns(3,4)P_2, and the product if its catalysis PtdIns(3)P have been demonstrated to play critical roles in lysosomal function (Ebner et al., 2019; Inpanathan and Botelho, 2019). For instance, PtdIns(3,4)P_2 can repress mTORC1 function on lysosomes and influence the highly motile properties of lysosomes such as anterograde (i.e. to the cell periphery) and retrograde (i.e. to the perinuclear area) transport (Bartolomeo et al., 2017; Marat et al., 2017; Munson et al., 2015). Knockdown of the PtdIns(3)P phosphatase MTMR4 has also been shown to increase lysosomal PtdIns(3)P levels and inhibit the nuclear translocation of TFEB without affecting mTORC1 (Pham et al., 2018).

Our findings highlight a novel route to LSC maintenance controlled by INPP4B and its role in lysosomal function. Further studies are required to explain the specific molecular underpinnings of INPP4B in lysosomal signalling. Nevertheless, these new data provide a basis for the utility of INPP4B as a biomarker of aggressive disease, explain its function in promoting AML aggressiveness and provide a rationale to explore INPP4B and its associated function in lysosome biology as novel strategies to target LSC and AML.

Acknowledgments

We thank all current and past members of the Salmena and Minden labs for technical assistance and critical discussions. We specifically thank Norman Iscove for technical advice; Johannes Zuber for *pMSCV-MLL-AF9-IRES-mVenus* plasmid; Lev Kats for invaluable advice; Robert C. Laister for encouraging deliberations and technical support. L.S. is the recipient of a Tier II Canada Research Chair and was supported through the Human Frontier Career Development Program Award. This work was supported in part by funds from the Department of Pharmacology and Toxicology and Temerty Faculty of Medicine, University of Toronto and awards from Canada Foundation for Innovation; The Natural Sciences and Engineering Research Council of Canada (RGPIN-2015-03984); Leukemia and Lymphoma Society of Canada (Operating Grant #317359; Operating Grant #422332); Acute Leukemia Translational Research Initiative through funding provided by the Ontario Institute for Cancer Research and Government of Ontario; Leukemia Research Foundation (New Investigator Award #169456), and Canadian Institutes for Health Research (Operating Grant #149032; Operating Grant #399716) awarded to L.S. In part by funds from Canadian Institutes for Health Research funds (MOP# 123343) awarded to J.V. Computational analyses were supported in part by funds from Natural Sciences Research Council (NSERC #203475), Canada Foundation for Innovation (CFI #225404, #30865), Ontario Research Fund (RDI #34876), IBM and Ian Lawson van Toch Fund awarded to I.J. R.J.B. is a recipient of a Tier II Canada Research Chair, and this work was supported in part by the Natural Sciences and Engineering Research Council of Canada (RGPIN-2015-05489 and RGPIN-2020-043343).

Author Contributions

J.F.W., K.C., G.G., D.K.C.L., G.T.S., E.M.S., S.Z.X. M.H.S., R.H., A.R. and L.S. performed experiments. D.K.C.L., M.G., M.K., I.D. and I.J. performed bioinformatic analyses. J.V. generated *Inpp4b* mouse models. J.E.D., R.B., and M.D.M. provided critical reagents, mentorship and expertise. J.F.W. and L.S. conceived and planned the study. J.F.W. and L.S. conceived the project and wrote the paper. L.S. secured funding for this study.

Declaration of Interests

All other authors declare no competing interests.

Figure Titles and Legends

Figure 1. Expression of *INPP4B* in hematopoietic cell lineages. A. Relative expression of *INPP4B* in human hematopoietic stem and progenitor cells (data mined from (Laurenti et al., 2015)). **B**. Relative expression of *Inpp4b* in murine hematopoietic stem and progenitor cells (data mined from Lara-Astiaso et al. 2014). **C**. Schematic depicting *INPP4B* expression in the haematopoietic hierarchy (high = dark blue, low = light blue). **D**. Representative pseudocolour dot-plot and contour plot from immunophenotyping of the adult bone marrow niche in *Inpp4b*$^{+/+}$ and *Inpp4b*$^{-/-}$ mice (*n*=6). **E.** Bone marrow stem cell fractions from age- and sex-matched adult *Inpp4b*$^{+/+}$ and *Inpp4b*$^{-/-}$ mice shown as a percentage of total bone marrow monocuclear cells. **F**. Bone marrow progenitor fractions from age- and sex-matched adult *Inpp4b*$^{+/+}$ and *Inpp4b*$^{-/-}$ mice, shown as a percentage of total bone marrow monocuclear cells.

Figure 2. *Inpp4b*-deficiency reduces colony formation and repopulation capacity of hematopoietic progenitors. A. Total colony counts from weekly serial replating of total bone marrow from age- and

sex-matched *Inpp4b*$^{+/+}$ and *Inpp4B*$^{-/-}$ mice (*n*=6, ±S.E.M.). **B**. Kaplan-Meier survival analysis after serial myeloablation (5'-fluorouracil, weekly i.p.) of age- and sex-matched *Inpp4b*$^{+/+}$ and *Inpp4B*$^{-/-}$ mice (*n*=10). **C.** Cell cycle analysis in sorted LSK cells, 48 hours after acute myeloablation with single 5'-fluorouracil treatment, measured by intracellular Ki67 level and flow cytometry. **D.** Relative contribution of *Inpp4b*$^{+/+}$, *Inpp4b*$^{+/-}$ and *Inpp4b*$^{-/-}$ long term HSCs to the regeneration of the myeloid populations in three consecutive competitive transplant experiments (*n*=10, ±S.E.M.). **E.** Relative contribution of *Inpp4b*$^{+/+}$, *Inpp4b*$^{+/-}$ and *Inpp4b*$^{-/-}$ long term HSCs to the regeneration of the total and myeloid CD45.1 (competitor) and CD45.2 (donor) populations in competitive transplant experiments at 20 weeks and 64 weeks (*n*=10, ±S.E.M.)

Figure 3. *INPP4B* expression is associated with leukemic stem cells in human AML. **A**. Relative expression of *INPP4B* from 227 AML patient-derived samples sorted based on the expression of combinations of CD34 and CD38 surface markers (Ng et al., 2016). **B.** Relative *INPP4B* expression in 278 sorted fractions characterized as LSC^{+} and LSC^{-} enriched by their engraftment potential into NOD/SCID mice (Ng et al., 2016). **C**. Gene set enrichment analysis (GSEA) of the LSC-17 gene set in *INPP4B* sorted AML patient samples (Ng et al., 2016) across 6 AML public patient datasets.

Figure 4. *Inpp4b*-deficient *MLL-AF9* cells have a decreased leukemogenic potential and have a more differentiated phenotype. **A.** Kaplan-meier survival analysis of primary Venus^{+}-*MLL-AF9* leukemias generated from *Inpp4b*$^{+/+}$ and *Inpp4B*$^{-/-}$ mouse LSK cells (*n*=10). **B.** Kaplan-meier survival analysis of secondary *MLL-AF9* leukemias generated by transplantation of cells from *Inpp4b*$^{+/+}$ and *Inpp4b*$^{-/-}$ *MLL-AF9* leukemia blasts (*n*=6). **C.** Limiting dilution assay (LDA) of *Inpp4b*$^{+/+}$ (dark blue (*n*=12)) and *Inpp4b*$^{-/-}$ *MLL-AF9* (light blue (*n*=12)) leukemia cells (1000, 250, 100, and 25 cells) into host wild-type C57BL/6 mice. **D.** Representative image of type-I and type-II colonies from secondary *MLL-AF9* leukemia cells (left). Total and percentage colony counts in LFC assays from *Inpp4b*$^{+/+}$ and

Inpp4B$^{-/-}$ murine *MLL-AF9* leukemia blasts (*n*=8, ±S.E.M.; right). **E**. Representative images of undifferentiated and differentiated blasts from *Inpp4b*$^{+/+}$ and *Inpp4b*$^{-/-}$ *MLL-AF9* terminal leukemias (*n*=3, ±S.E.M.; left). Proportion of undifferentiated and differentiated leukemic blasts from *Inpp4b*$^{+/+}$ (right). **F.** Representative density plots of surface marker expression on *Inpp4b*$^{+/+}$ and *Inpp4B*$^{-/-}$ *MLL-AF9* leukemia blasts. **G**. Fraction of *Inpp4b*$^{+/+}$ and *Inpp4b*$^{-/-}$ CD45^{+} *MLL-AF9* leukemia blasts expressing various surface markers (*n*=3, ±S.E.M.).

Figure 5. *Inpp4b* expression is associated with lysosomal gene sets. **A**.Top 20 enriched KEGG gene sets in *Inpp4b*$^{+/+}$ and *Inpp4b*$^{-/-}$ *MLL-AF9* leukemia blast cells determined using GSEA. **B.** Top 20 pathways from InnateDB Gene Ontology (GO) over-representation analysis (ORA) of all genes with significantly altered expression in *Inpp4b*$^{+/+}$ and *Inpp4b*$^{-/-}$ MLL-AF9 leukemia blast cells (Breuer et al., 2013). **C.** Heat map of differentially expressed KEGG Lysosome genes from *Inpp4b*$^{+/+}$ and *Inpp4b*$^{-/-}$ *MLL-AF9* leukemia blast cells (upregulated in red, downregulated in blue). **D.** STRING-db analysis of differential expression of KEGG Lysosome genes from *Inpp4b*$^{+/+}$ and *Inpp4b*$^{-/-}$ *MLL-AF9* leukemia blast cells. **E-F.** Gene set expression analysis (GSEA) for Lysosome pathway genes in *Inpp4b*$^{-/-}$ *MLL-AF9* leukemia blast cells with E. KEGG Lysosome gene set; F. Lysosomal proteins gene set ((Sardiello et al., 2009)); G. LSC17 signature gene set ((Mootha et al., 2003; Ng et al., 2016; Subramanian et al., 2005)).

Figure 6: A Lysosome gene set is enriched in patients with low levels of INPP4B. **A-B**. Scatter plot of the top 20 enriched KEGG gene sets in *INPP4B*-low patients from the **A.** TCGA and **B.** Verhaak dataset. **C-F.** GSEA plots for the KEGG lysosome gene set in *INPP4B*-low patients from the C. TCGA AML; D. Verhaak AML; E. Valk AML; F. Wouters AML dataset. **G.** Venn diagram illustrating the genes from the KEGG lysosome gene set that contribute to the leading-edge subset in the four AML datasets. **H.** Table of the common core enriched lysosome genes among the four AML datasets.

Figure 7: INPP4B regulates lysosomal biology. **A.** Representative immunoblot and micrograph of INPP4B expression in U2OS cells upon INPP4B induction with doxycycline (100mg/mL). **B.** Representative immunoblot and micrograph of INPP4B expression in U2OS upon treatment with siRNA targeting *INPP4B* or control siRNA. **C.** Representative micrograph of LAMP1 dispersion across perinuclear shells (1-4) in U2OS cells. **D.** Quantification of LAMP1 puncta in perinuclear shells (1-4) in U2OS cells upon INPP4B induction or siRNA-mediated knockdown of INPP4B. **E.** Quantification of LAMP1 puncta and total cellular LAMP1 staining intensity in U2OS upon treatment with small interfering RNA targeting *INPP4B* or a non-specific control. **F-G.** Representative micrograph and quantification of lysosomal proteolytic function as measured by (DQ)-BSA-Green™ fluorescence relative to Dextran-Red in U2OS cells upon INPP4B induction with doxycycline or siRNA-mediated knockdown of INPP4B.

Figure 8: INPP4B regulates lysosomal biology in leukemia cells. **A.** Inducible-INPP4B OCI-AML2 cells were treated without or with doxycycline (100mg/mL) and incubated with DQ-BSA-Green™ and fluorescence was monitored by flow cytometry hourly, for up to 6 hours. **B.** *Inpp4b*$^{+/+}$ and *Inpp4B*$^{-/-}$ *MLL-AF9* leukemia blasts were incubated with DQ-BSA-Green™ and fluorescence was monitored by flow cytometry hourly, for up to 8 hours. **C.** *Inpp4b*$^{+/+}$ and *Inpp4B*$^{-/-}$ *MLL-AF9* leukemia blasts were plated in the CFC assay in the presence of Lys05 for 7 days. Violin/dot plots represent normalized colony counts. **D.** *Inpp4b*$^{+/+}$ *MLL-AF9* leukemia blasts were plated in the LFC assay in the presence of Lys05 for 5 days.

Methods

Immunophenotyping of *Inpp4b*$^{-/-}$ mice. Total bone marrow was extracted from the hind legs of *Inpp4b*$^{+/+}$, *Inpp4b*$^{+/-}$ and *Inpp4b*$^{-/-}$ mice by crushing into ice-cold Iscove's Modified Dulbecco's Medium (IMDM) medium. RBC lysis was performed using standard ammonium chloride procedure. Total bone marrow mononuclear cell (MNCs) was stained for surface marker expression in PBS. 2mM EDTA, 2% FBS for 90 minutes at 4°C. The following antibody cocktails were used: anti-mouse CD3 (145-2C11), anti-mouse CD45R/B220 (RA3-6B2, anti-mouse CD11b (M1/70), anti-mouse Erythroid marker (TER-119), anti-mouse Ly-6G (RB6-8C5), anti-mouse CD34 (RAM34), anti-mouse Flk2 (A2F10), anti-mouse c-kit (2B8), anti-mouse Sca1 (D7), anti-mouse CD150 (TC15-12F12.2), anti-mouse CD48 (HM48-1), anti-mouse CD201/EPCR (eBio1560). All antibodies were obtained from eBiosciences, BD Pharmingen or Biolegend. Cells were analysed on a LSR Fortessa X20 (BD Biosciences).

***MLL-AF9* AML Models.** *MLL-AF9* expressing cells were generated by retroviral transduction of murine bone marrow progenitors. Briefly, bone marrow was flushed from the long bones of 10-week-old *Inpp4b*$^{+/+}$ and *Inpp4b*$^{-/-}$ mice. From these total bone marrow preparations, 2 x 10^6 LSK cells were sorted and grown for 24 hours in IMDM supplemented with 20 ng/ml SCF, 10 ng/ml IL-6 and 10 ng/ml IL-3 (Gibco). *Inpp4b*$^{+/+}$ and *Inpp4b*$^{-/-}$ LSK were each retrovirally transduced with pMSCV-*MLL-AF9*-IRES-mVenus. 24 hours post retroviral transduction, 2 x 10^5 Venus$^+$ cells were transplanted to sub-lethally irradiated (4.5Gy) donor C57BL/6 mice to generate primary leukemias (Zuber et al., 2009). Subsequent transplantation of mVenus$^+$ cells from mice with terminal leukemias were designated as secondary leukemia assays. *In vitro* assays were performed in IMDM medium with 2% methylcellulose, supplemented with 20 ng/ml SCF, 10 ng/ml IL-6 and 10 ng/ml IL-3 (Stem Cell Technologies). Cytological analysis of blood and bone marrow smears from *Inpp4b*$^{+/+}$ and *Inpp4b*$^{-/-}$ leukemic mice was done by classical wright-giemsa staining (Sigma). For limiting dilution transplantation assays (LDA),

MLL-AF9 leukemia cells were injected at defined doses (equivalent to 10, 25, 50, 100, and 1000 blast cells) into 8-week-old female C57BL/6 mice. LSC frequency was estimated using the online tool ELDA (http://bioinf.wehi.edu.au/software/elda/index.html) ((Hu and Smyth, 2009).

Competitive Transplant of *Inpp4b*$^{-/-}$ bone marrow. Lethally irradiated C57BL/6-CD45.1 congenic mice were reconstituted with bone marrow MNCs from age- and sex-matched *Inpp4b*$^{+/+}$ or *Inpp4b*$^{-/-}$ mice (CD45.2), in competition with bone marrow MNCs from C57BL/6-CD45.1 mice. Competitive transplants were carried out in a 1:1 ratio, with 1 x 10^6 cells from each combined prior to injection. Reconstitution of donor-derived cells (CD45.2) was monitored by staining blood cells with mAbs against CD45.2, CD45.1, Mac-1, and Gr-1. For the serial transplantation analysis, bone marrow cells (1 × 10^6) were obtained from recipient mice at 20 weeks post-transplantation and transplanted into a second set of lethally irradiated mice. The ratio of 1:1, Cd45.1:CD45.2 was re-established prior to secondary transplant. Subsequent transplants were performed in the same manner.

Gene expression data. Genome-wide expression data from The Cancer Genome Atlas (TCGA)-LAML dataset was downloaded from the ICGC database (https://icgc.org/). Normalized microarray data from the Herold (GSE37642-GPL570), Klein (GSE15434), Metzeler (GSE12417-GPL570), Valk (GSE1159), Verhaak (GSE6891), Wouters (GSE14468), Laurenti (GSE42414, GPL14951), Notta (GSE76234), Novershtern (GSE24759), Pietras (GSE68529), Rapin (GSE42519) and Lara-Asiato (GSE60101) datasets were downloaded from the GEO database (https://www.ncbi.nlm.nih.gov/geo/).

***In vitro* CFU Assays of *Inpp4b*$^{-/-}$ bone marrow.** To determine the re-plating ability of HSPCs *Inpp4b*$^{+/+}$ and *Inpp4b*$^{-/-}$ we plated bone marrow from age- and sex-matched mice in Methocult GF M3434 (Stem Cell Technologies) according to the manufacturer's instructions. Briefly, total mouse bone

marrow MNCs were flushed from long bones into IMDM medium. RBCs were lysed in ammonium chloride solution and cells were resuspended in IMDM. 2 x 10^4 cells were plated onto 35-mm dishes and incubated at 37°C, 5% CO_2 for 7-days. After 7-days colonies were counted and scored. 2 x 10^4 cells were re-plated onto fresh methocult every 7 days and counted, until exhaustion.

5'-FU Treatment. Age- and sex-matched *Inpp4b*$^{+/+}$ or *Inpp4b*$^{-/-}$ mice were treated with 5'-FU (150mg/kg in saline, i.p.) or saline control, once weekly. Survival analysis was performed by the Kaplan-Meier method. Necropsies were performed and extracted spleens were weighed. Separately, LSK cells were sorted 48-hours after treatment with a single dose of 5'-FU from age- and sex-matched *Inpp4b*$^{+/+}$ and *Inpp4b*$^{-/-}$ mice. These LSK cells were then fixed, and cycling was assessed by flow cytometry measurement of Ki67 levels.

Blood Analysis. Total blood counts for Age- and sex-matched *Inpp4b*$^{+/+}$ and *Inpp4b*$^{-/-}$ mice (*n*=10) were performed using a VetScan HM5 (Abaxis) by the Division of Comparative Medicine (University of Toronto).

Mass Cytometry. Purified mAbs were conjugated with heavy metals by the Flow and Mass Cytometry Facility, The Hospital for Sick Children. Murine AML blasts were counted and 2 x10^6 cells for each sample were stained for cell surface markers in staining media (PBS containing 1% BSA and 0.02% NaN3) for 30 minutes at 4C. Cells were washed with protein-free PBS, stained with 1 mmol/L cisplatin for 5 minutes at room temperature, fixed using the transcription factor buffer set (BD Biosciences) followed by intracellular staining for 60 minutes at 4C. Cells were washed with staining media and

stained with 100 nmol/L iridium-labeled DNA-intercalator (Fluidigm) in PBS containing 0.3% saponin and 1.6% formaldehyde at 4 C for up to 48 hours. Cells were washed twice with deionized water prior to adding EQ normalization beads containing Ce140, Eu151, Eu153, Ho165, and Lu175 (Fluidigm) and acquiring on a Helios mass cytometer by The Flow and Mass Cytometry Facility, The Hospital for Sick Children. After normalizing and randomizing values near zero using the Helios software, FCS files were uploaded to Cytobank for analysis.

RNA sequencing. *Inpp4b*$^{+/+}$ or *Inpp4b*$^{-/-}$ *MLL-AF9* leukemias (3 in total for each genotype) were sorted for Venus+ before isolation of total cellular RNA with a RNeasy isolation kit (Qiagen). A Bioanalyzer 2100 (Agilent) was used for quality control and quantification. Illumina MouseRef-8 v2.0 Expression BeadChip kits were used for genome-wide expression profiling according to standard protocols at The Centre for Applied Genomics core facility at the Hospital for Sick Children. R Bioconductor 2.13.0 software was used for data processing and other statistical analyses. Raw signals from 25,697 probes were pre-processed for background subtraction, quantile normalization and log2 transformation before the use of moderated t-tests from the Bioconductor software package Limma (linear models for microarray data). Empirical Bayes smoothing was applied to the standard errors. Paired t-tests were used for the identification of differentially expressed genes expression in each genotype subset, and the false-discovery rate (FDR) was estimated with the Benjamini-Hochberg method to correct for multiple testing. Pearson correlations showed that technical replicates had very high correlations between chips. For genes represented by multiple probes sets on the array, we selected the ones with the highest ANOVA F-statistics (lowest FDR-adjusted q value).

Bioinformatics

Gene Set Enrichment Analysis (GSEA). GSEA was performed on the datasets using GSEA v.4.0.3 provided by the Broad Institute (http://software.broadinstitute.org/gsea/downloads.jsp). Samples were rank ordered and split by INPP4B status, 25% high/75% low (human) or *Inpp4b*$^{+/+}$/*Inpp4b*$^{-/-}$ (mouse). Enriched gene sets were identified by 1,000 phenotype permutations in the human datasets, and 1,000 gene set permutations in the mouse dataset. Gene sets with a nominal *p*--value < 0.05 were considered significantly enriched. The curated KEGG (CP: KEGG) and BROWN_MYLEOID_CELL_DEVELOPMENT_UP gene set were obtained from MSigDB Collections (http://software.broadinstitute.org/gsea/msigdb/collections.jsp) and the LSC17 and Lysosomal Proteins gene sets were generated from the indicated publication (Ng et al., 2016; Palmieri et al., 2011).

Gene Ontology (GO). GO analysis was performed using the InnateDB database (https://www.innatedb.ca/; Breuer et al., 2013).

Gene Network Analysis. The lysosome interacting genes were passed through String-db.v.11 (Szklarczyk et al. 2019). and the combined binding score for each protein-protein interaction was obtained. This output, which is experimentally determined and annotated, connects the protein nodes. The absolute log fold change from the RNAseq is used to size the nodes and the colour corresponds to the -$\log_{10}$(Pvalue). The interaction map was generated by 'ForceAtlas2' in Gephi.v.0.9.2. (Jacomy et al. 2014)

Immunofluorescence and DQ-BSA assays in U2OS cells

For LAMP1 immunofluorescence, U2OS cells were fixed with ice-cold methanol (100%) for 5 min at -20 C. Cells were then washed with PBS and incubated for 1 h in blocking buffer (10% FBS, 3% BSA in PBS) before the addition of antibody. Anti-LAMP1 rabbit XP® monoclonal antibodies (1:100, Clone D2D11, Cell Signaling) were added to cells in blocking buffer and incubated for 1 h at room temperature. Secondary anti-rabbit antibodies were then added to cells at a 1:1000 dilution in blocking buffer and incubated for 1 h at room temperature. After the indicated time, cells were stained with 1

μg/mL DAPI (Roche Biochemicals). Cells were washed three times with 0.3% BSA in PBS between each step and washed a final time before mounting coverslips with Dako fluorescent mounting medium. Z-stacks of cells were acquired at 0.3 μm interval steps with a Quorum DisKovery Spinning Disc confocal microscope system equipped with a Leica DMi8 microscope connected to Andor Zyla 4.2 Megapixel sCMOS camera and controlled by Quorum Wave FX Powered by MetaMorph software (Quorum Technologies, Guelph, ON). LAMP1 puncta, fluorescence intensity, and positioning were quantified using ImageJ software. For lysosome positioning, each cell was outlined manually to generate a region of interest (shell), and the same shell was reduced in size by 15-pixel iterations to produce four shells in total per cell. In all cases, thresholding for lysosomal signal was conducted manually followed by particle detection analysis (particles with a minimum area of 2 pixel) and fluorescence intensity for each shell and normalized to shell area. Images obtained from randomly selected 60 cells from 3 independent experiments. To measure the proteolytic capacity of lysosomes, cells were treated with 10 μg/mL DQ Green BSA (Invitrogen) and 2 μM fixable Alexa-647-conjugated 10 kDa dextran (Invitrogen) for 6 h, followed by a 1h chase in label-free media. Following a chase period, cells were fixed in 4% PFA for 20 min and imaged. DQ-BSA and Alexa-647-dextran images were acquired using an Olympus IX83 microscope system with a Hamamatsu ORCA-Flash4.0 digital camera controlled by CellSens Dimensions software (Olympus Canada Inc., Richmond Hill, ON). Images obtained from randomly selected 60 cells from 3 independent experiments were quantified by using ImageJ. In all cases, thresholding for DQ Green BSA and dextran signals were conducted manually followed by fluorescence intensity for the whole cell. The mean intensity of the whole cell was obtained by drawing an area covering the whole cell. Subsequently fluorescent intensities were quantified by normalizing the DQ-BSA fluorescence signal against the Alexa-647 signal after background correction.

DQ-BSA in *MLL-AF9* cells. *MLL-AF9* Inpp4b+/+ and Inpp4b-/- cells were cultured for 48h and AML2-TETON-INPP4B cells were treated with doxycycline (100ng/mL) prior to lysosome labelling. Cells were incubated with 10ug/mL DQ Red BSA (Invitrogen) or 2uM Alexa-647-conjugated 10kDa dextran (Invitrogen) in complete media for 1h to 6h at 37°C. At each time point, cells were washed twice with PBS and subsequently analyzed for whole cell fluorescence with Beckman Coulter Cytoflex flow cytometer. A total of 60,000 events were collected per sample per time point using the APC channel. Non-labeled cells were used as control for determining background signal and as time point 0.

Lysosome labelling. U2OS lysosomes were labelled by incubating with Lucifer yellow 2.5 mg/ml (Thermo Fisher Scientific, Mississauga, ON) for 4 h in complete media at 37^{o}C and 5% CO_2. Cells were washed twice with phosphate-buffered saline (PBS) and supplemented with complete media for 1 h.

Spinning disc confocal microscopy. Imaging performed through spinning disc confocal microscopy with an Olympus IX81 inverted microscope equipped with a Hamamatsu C9100-13 EMCCD camera controlled by Volocity 6.3.0 (PerkinElmer, Bolton, ON). Time lapse live imaging was performed at single z-focal planes using complete media in a 5% CO_2 chamber at 37^{0}C.

Image analysis. To analyze the lysosome associated to cytosol ratio of INPP4B-mCherry, images imported to ImageJ, and 5-pixel wide lines measuring 40-pixel in length were designated to nucleus-excluded areas of the cell. Intensity plot profiles acquired and exported to excel spreadsheet, and values assorted according to intensity. Ratio obtained of highest 10 pixels over lowest 10 pixels (F_H/F_L

fluorescent ratio) where intensity signal-values representing cytosolic distribution was expected to have a ratio value of approximately 1.

Lentivirus production and generating TMEM192-3xHA stable cells. HEK293T cells were transfected with FuGene HD (Promega, Madison, WI) for pLJC5-TMEM192-3xHA (addgene) in combination with VSV-G and psPAX2 packaging plasmids to generate lentivirus. Media was replaced 24 h post transfection with fresh complete media for 48 h. Virus containing media was collected, and cells were supplemented with fresh complete media for 24 h followed by collection of virus containing media. Virus containing media was centrifuged at 1000 rpm for 3 min to remove cells and stored at -80^{0}C. To generate U2OS cells stably expressing TMEM192-3xHA, 1 million U2OS cells plated in 10 cm plates were overlayed with two 24 h rounds of 10 ml virus containing media supplemented with 8 µg/ml protamine sulfate. Virus containing media was replaced with fresh complete media for 24 h followed by 48 h selection with 2 µg/ml puromycin.

Lysosome immunoprecipitation. ~30 million cells plated in 15 cm plates were washed with PBS and collected through trypsinization. Cells were washed twice at 1000 x g for 2 min with 1 ml of KPBS (136 mM KCl, 10 mM KH_2PO_4, pH adjusted to 7.25 with KOH). Cell pellets resuspended and 20 µl collected, lysed with RIPA buffer and stored at -20^{0}C as input. The remaining 980 µl of cells were homogenized with 25 strokes of a 7 ml homogenizer. The homogenate was centrifuged 1000 x g for 2 min. The supernatant containing organelles was collected and incubated with 100 µl of KPBS prewashed anti-HA magnetic beads for 15 min on a gentle rotating shaker. The immunoprecipitates were washed four times with KPBS buffer on DynaMag-2 Spin Magnet (Thermo Fisher Scientific, Mississauga, ON). The immunoprecipitates and input were subjected to immunoblotting with the

following primary antibodies: Rabbit monoclonal antibody for INPP4B (1:1000, 14543, Cell Signaling) and HA (1:1000, 3724, Cell Signaling), Rabbit polyclonal antibody for VAPB (1:2000, HPA013144, Sigma, Oakville, ON), and Rabbit monoclonal antibody for LAMP1 (1:1000, 9091, Cell Signaling).

Quantification and Statistical Analysis

Errors bars show standard error of the mean (SEM). Data were analyzed with a two-tailed Student t-test for comparison of the means of two groups and by one-way ANOVA. P values of less than 0.05 were considered statistically significant. No randomization of mice or 'blinding' of researchers to sample identity was used during the analyses. Sample sizes were not predetermined on the basis of expected effect size, but rough estimations were made on the basis of pilot experiments and measurements. No data exclusion was applied.

References

The Cancer Genome Atlas Network (2012). Comprehensive molecular portraits of human breast tumours. Nature *490*, 61–70.

The Cancer Genome Atlas Research Network, Ley, T.J., Miller, C., Ding, L., Raphael, B.J., Mungall, A.J., Robertson, A.G., Hoadley, K., Triche, T.J., Laird, P.W., et al. (2013). Genomic and epigenomic landscapes of adult de novo acute myeloid leukemia. N. Engl. J. Med. *368*, 2059–2074.

Bibliography

Amaravadi, R.K., and Winkler, J.D. (2012). Lys05: a new lysosomal autophagy inhibitor. Autophagy *8*, 1383–1384.

Bagshaw, R.D., Mahuran, D.J., and Callahan, J.W. (2005a). A proteomic analysis of lysosomal integral membrane proteins reveals the diverse composition of the organelle. Mol. Cell. Proteomics *4*, 133–143.

Bagshaw, R.D., Mahuran, D.J., and Callahan, J.W. (2005b). Lysosomal membrane proteomics and biogenesis of lysosomes. Mol. Neurobiol. *32*, 27–41.

Balgobind, B.V., Van den Heuvel-Eibrink, M.M., De Menezes, R.X., Reinhardt, D., Hollink, I.H.I.M., Arentsen-Peters, S.T.J.C.M., van Wering, E.R., Kaspers, G.J.L., Cloos, J., de Bont, E.S.J.M., et al. (2011). Evaluation of gene expression signatures predictive of cytogenetic and molecular subtypes of pediatric acute myeloid leukemia. Haematologica *96*, 221–230.

Bartolomeo, R., Cinque, L., De Leonibus, C., Forrester, A., Salzano, A.C., Monfregola, J., De Gennaro, E., Nusco, E., Azario, I., Lanzara, C., et al. (2017). mTORC1 hyperactivation arrests bone growth in lysosomal storage disorders by suppressing autophagy. J. Clin. Invest. *127*, 3717–3729.

Breuer, K., Foroushani, A.K., Laird, M.R., Chen, C., Sribnaia, A., Lo, R., Winsor, G.L., Hancock, R.E.W., Brinkman, F.S.L., and Lynn, D.J. (2013). InnateDB: systems biology of innate immunity and beyond--recent updates and continuing curation. Nucleic Acids Res. *41*, D1228-33.

Cabukusta, B., and Neefjes, J. (2018). Mechanisms of lysosomal positioning and movement. Traffic *19*, 761–769.

Callahan, J.W., Bagshaw, R.D., and Mahuran, D.J. (2009). The integral membrane of lysosomes: its proteins and their roles in disease. J. Proteomics *72*, 23–33.

Cancer Genome Atlas Research Network, Ley, T.J., Miller, C., Ding, L., Raphael, B.J., Mungall, A.J., Robertson, A.G., Hoadley, K., Triche, T.J., Laird, P.W., et al. (2013). Genomic and epigenomic landscapes of adult de novo acute myeloid leukemia. N. Engl. J. Med. *368*, 2059–2074.

Cechakova, L., Ondrej, M., Pavlik, V., Jost, P., Cizkova, D., Bezrouk, A., Pejchal, J., Amaravadi, R.K., Winkler, J.D., and Tichy, A. (2019). A potent autophagy inhibitor (lys05) enhances the impact of ionizing radiation on human lung cancer cells H1299. Int. J. Mol. Sci. *20*.

Chi, M.N., Guo, S.T., Wilmott, J.S., Guo, X.Y., Yan, X.G., Wang, C.Y., Liu, X.Y., Jin, L., Tseng, H.-Y., Liu, T., et al. (2015). INPP4B is upregulated and functions as an oncogenic driver through SGK3 in a subset of melanomas. Oncotarget *6*, 39891–39907.

Dick, J.E. (2008). Stem cell concepts renew cancer research. Blood *112*, 4793–4807.

Dzneladze, I., He, R., Woolley, J.F., Son, M.H., Sharobim, M.H., Greenberg, S.A., Gabra, M., Langlois, C., Rashid, A., Hakem, A., et al. (2015). INPP4B overexpression is associated with poor clinical outcome and therapy resistance in acute myeloid leukemia. Leukemia *29*, 1485–1495.

Dzneladze, I., Woolley, J.F., Rossell, C., Han, Y., Rashid, A., Jain, M., Reimand, J., Minden, M.D., and Salmena, L. (2018). SubID, a non-median dichotomization tool for heterogeneous populations, reveals the pan-cancer significance of INPP4B and its regulation by EVI1 in AML. PLoS ONE *13*, e0191510.

Ebner, M., Koch, P.A., and Haucke, V. (2019). Phosphoinositides in the control of lysosome function and homeostasis. Biochem. Soc. Trans. *47*, 1173–1185.

Eppert, K., Takenaka, K., Lechman, E.R., Waldron, L., Nilsson, B., van Galen, P., Metzeler, K.H., Poeppl, A., Ling, V., Beyene, J., et al. (2011). Stem cell gene expression programs influence clinical outcome in human leukemia. Nat. Med. *17*, 1086–1093.

Estey, E., and Döhner, H. (2006). Acute myeloid leukaemia. Lancet *368*, 1894–1907.

Ferron, M., Boudiffa, M., Arsenault, M., Rached, M., Pata, M., Giroux, S., Elfassihi, L., Kisseleva, M., Majerus, P.W., Rousseau, F., et al. (2011). Inositol polyphosphate 4-phosphatase B as a regulator of bone mass in mice and humans. Cell Metab. *14*, 466–477.

García-Prat, L., Kaufmann, K.B., Schneiter, F., Voisin, V., Murison, A., Chen, J., Chan-Seng-Yue, M., Gan, O.I., McLeod, J.L., Smith, S.A., et al. (2021). Dichotomous regulation of lysosomes by MYC and TFEB controls hematopoietic stem cell fate. BioRxiv.

Gasser, J.A., Inuzuka, H., Lau, A.W., Wei, W., Beroukhim, R., and Toker, A. (2014). SGK3 mediates INPP4B-dependent PI3K signaling in breast cancer. Mol. Cell *56*, 595–607.

Grimwade, D., Hills, R.K., Moorman, A.V., Walker, H., Chatters, S., Goldstone, A.H., Wheatley, K., Harrison, C.J., Burnett, A.K., and National Cancer Research Institute Adult Leukaemia Working Group (2010). Refinement of cytogenetic classification in acute myeloid leukemia: determination of prognostic significance of rare recurring chromosomal abnormalities among 5876 younger adult patients treated in the United Kingdom Medical Research Council trials. Blood *116*, 354–365.

Guo, S.T., Chi, M.N., Yang, R.H., Guo, X.Y., Zan, L.K., Wang, C.Y., Xi, Y.F., Jin, L., Croft, A., Tseng, H.Y., et al. (2016). INPP4B is an oncogenic regulator in human colon cancer. Oncogene *35*, 3049–3061.

Herold, T., Jurinovic, V., Batcha, A.M.N., Bamopoulos, S.A., Rothenberg-Thurley, M., Ksienzyk, B., Hartmann, L., Greif, P.A., Phillippou-Massier, J., Krebs, S., et al. (2018). A 29-gene and cytogenetic score for the prediction of resistance to induction treatment in acute myeloid leukemia. Haematologica *103*, 456–465.

Hu, Y., and Smyth, G.K. (2009). ELDA: extreme limiting dilution analysis for comparing depleted and enriched populations in stem cell and other assays. J. Immunol. Methods *347*, 70–78.

Inpanathan, S., and Botelho, R.J. (2019). The lysosome signaling platform: adapting with the times. Front. Cell Dev. Biol. *7*, 113.

Jin, H., Yang, L., Wang, L., Yang, Z., Zhan, Q., Tao, Y., Zou, Q., Tang, Y., Xian, J., Zhang, S., et al. (2018). INPP4B promotes cell survival via SGK3 activation in NPM1-mutated leukemia. J. Exp. Clin. Cancer Res. *37*, 8.

Jung, N., Dai, B., Gentles, A.J., Majeti, R., and Feinberg, A.P. (2015). An LSC epigenetic signature is largely mutation independent and implicates the HOXA cluster in AML pathogenesis. Nat. Commun. *6*, 8489.

Klein, H.-U., Ruckert, C., Kohlmann, A., Bullinger, L., Thiede, C., Haferlach, T., and Dugas, M. (2009). Quantitative comparison of microarray experiments with published leukemia related gene expression signatures. BMC Bioinformatics *10*, 422.

Klepin, H.D., Rao, A.V., and Pardee, T.S. (2014). Acute myeloid leukemia and myelodysplastic syndromes in older adults. J. Clin. Oncol. *32*, 2541–2552.

Kofuji, S., Kimura, H., Nakanishi, H., Nanjo, H., Takasuga, S., Liu, H., Eguchi, S., Nakamura, R., Itoh, R., Ueno, N., et al. (2015). INPP4B is a ptdins(3,4,5)p3 phosphatase that can act as a tumor suppressor. Cancer Discov. *5*, 730–739.

Korolchuk, V.I., Saiki, S., Lichtenberg, M., Siddiqi, F.H., Roberts, E.A., Imarisio, S., Jahreiss, L., Sarkar, S., Futter, M., Menzies, F.M., et al. (2011). Lysosomal positioning coordinates cellular nutrient responses. Nat. Cell Biol. *13*, 453–460.

Krivtsov, A.V., Twomey, D., Feng, Z., Stubbs, M.C., Wang, Y., Faber, J., Levine, J.E., Wang, J., Hahn, W.C., Gilliland, D.G., et al. (2006). Transformation from committed progenitor to leukaemia stem cell initiated by MLL-AF9. Nature *442*, 818–822.

Lara-Astiaso, D., Weiner, A., Lorenzo-Vivas, E., Zaretsky, I., Jaitin, D.A., David, E., Keren-Shaul, H., Mildner, A., Winter, D., Jung, S., et al. (2014). Immunogenetics. Chromatin state dynamics during blood formation. Science *345*, 943–949.

Laurenti, E., Doulatov, S., Zandi, S., Plumb, I., Chen, J., April, C., Fan, J.-B., and Dick, J.E. (2013). The transcriptional architecture of early human hematopoiesis identifies multilevel control of lymphoid commitment. Nat. Immunol. *14*, 756–763.

Laurenti, E., Frelin, C., Xie, S., Ferrari, R., Dunant, C.F., Zandi, S., Neumann, A., Plumb, I., Doulatov, S., Chen, J., et al. (2015). CDK6 levels regulate quiescence exit in human hematopoietic stem cells. Cell Stem Cell *16*, 302–313.

Lawrence, R.E., and Zoncu, R. (2019). The lysosome as a cellular centre for signalling, metabolism and quality control. Nat. Cell Biol. *21*, 133–142.

Lechman, E.R., Gentner, B., Ng, S.W.K., Schoof, E.M., van Galen, P., Kennedy, J.A., Nucera, S., Ciceri, F., Kaufmann, K.B., Takayama, N., et al. (2016). miR-126 Regulates Distinct Self-Renewal Outcomes in Normal and Malignant Hematopoietic Stem Cells. Cancer Cell *29*, 214–228.

Leeman, D.S., Hebestreit, K., Ruetz, T., Webb, A.E., McKay, A., Pollina, E.A., Dulken, B.W., Zhao, X., Yeo, R.W., Ho, T.T., et al. (2018). Lysosome activation clears aggregates and enhances quiescent neural stem cell activation during aging. Science *359*, 1277–1283.

Liang, R., Arif, T., Kalmykova, S., Kasianov, A., Lin, M., Menon, V., Qiu, J., Bernitz, J.M., Moore, K., Lin, F., et al. (2020). Restraining lysosomal activity preserves hematopoietic stem cell quiescence and potency. Cell Stem Cell *26*, 359-376.e7.

Li Chew, C., Lunardi, A., Gulluni, F., Ruan, D.T., Chen, M., Salmena, L., Nishino, M., Papa, A., Ng, C.,

Fung, J., et al. (2015). In Vivo Role of INPP4B in Tumor and Metastasis Suppression through Regulation of PI3K-AKT Signaling at Endosomes. Cancer Discov. *5*, 740–751.

Loeffler, D., Wehling, A., Schneiter, F., Zhang, Y., Müller-Bötticher, N., Hoppe, P.S., Hilsenbeck, O., Kokkaliaris, K.D., Endele, M., and Schroeder, T. (2019). Publisher Correction: Asymmetric lysosome inheritance predicts activation of haematopoietic stem cells. Nature *573*, E5.

Löwenberg, B., Downing, J.R., and Burnett, A. (1999). Acute myeloid leukemia. N. Engl. J. Med. *341*, 1051–1062.

Mandegar, M.A., Huebsch, N., Frolov, E.B., Shin, E., Truong, A., Olvera, M.P., Chan, A.H., Miyaoka, Y., Holmes, K., Spencer, C.I., et al. (2016). CRISPR Interference Efficiently Induces Specific and Reversible Gene Silencing in Human iPSCs. Cell Stem Cell *18*, 541–553.

Marat, A.L., Wallroth, A., Lo, W.-T., Müller, R., Norata, G.D., Falasca, M., Schultz, C., and Haucke, V. (2017). mTORC1 activity repression by late endosomal phosphatidylinositol 3,4-bisphosphate. Science *356*, 968–972.

McAfee, Q., Zhang, Z., Samanta, A., Levi, S.M., Ma, X.-H., Piao, S., Lynch, J.P., Uehara, T., Sepulveda, A.R., Davis, L.E., et al. (2012). Autophagy inhibitor Lys05 has single-agent antitumor activity and reproduces the phenotype of a genetic autophagy deficiency. Proc Natl Acad Sci USA *109*, 8253–8258.

Metzeler, K.H., Hummel, M., Bloomfield, C.D., Spiekermann, K., Braess, J., Sauerland, M.-C., Heinecke, A., Radmacher, M., Marcucci, G., Whitman, S.P., et al. (2008). An 86-probe-set gene-expression signature predicts survival in cytogenetically normal acute myeloid leukemia. Blood *112*, 4193–4201.

Mootha, V.K., Lindgren, C.M., Eriksson, K.-F., Subramanian, A., Sihag, S., Lehar, J., Puigserver, P., Carlsson, E., Ridderstråle, M., Laurila, E., et al. (2003). PGC-1alpha-responsive genes involved in oxidative phosphorylation are coordinately downregulated in human diabetes. Nat. Genet. *34*, 267–273.

Munson, M.J., Allen, G.F., Toth, R., Campbell, D.G., Lucocq, J.M., and Ganley, I.G. (2015). mTOR activates the VPS34-UVRAG complex to regulate autolysosomal tubulation and cell survival. EMBO J. *34*, 2272–2290.

Ng, S.W.K., Mitchell, A., Kennedy, J.A., Chen, W.C., McLeod, J., Ibrahimova, N., Arruda, A., Popescu, A., Gupta, V., Schimmer, A.D., et al. (2016). A 17-gene stemness score for rapid determination of risk in acute leukaemia. Nature *540*, 433–437.

Notta, F., Zandi, S., Takayama, N., Dobson, S., Gan, O.I., Wilson, G., Kaufmann, K.B., McLeod, J., Laurenti, E., Dunant, C.F., et al. (2016). Distinct routes of lineage development reshape the human blood hierarchy across ontogeny. Science *351*, aab2116.

Novershtern, N., Subramanian, A., Lawton, L.N., Mak, R.H., Haining, W.N., McConkey, M.E., Habib, N., Yosef, N., Chang, C.Y., Shay, T., et al. (2011). Densely interconnected transcriptional circuits control cell states in human hematopoiesis. Cell *144*, 296–309.

Palmieri, M., Impey, S., Kang, H., di Ronza, A., Pelz, C., Sardiello, M., and Ballabio, A. (2011). Characterization of the CLEAR network reveals an integrated control of cellular clearance pathways.

Hum. Mol. Genet. *20*, 3852–3866.

Perera, R.M., Di Malta, C., and Ballabio, A. (2019). Mit/tfe family of transcription factors, lysosomes, and cancer. Annu. Rev. Cancer Biol. *3*, 203–222.

Pham, H.Q., Yoshioka, K., Mohri, H., Nakata, H., Aki, S., Ishimaru, K., Takuwa, N., and Takuwa, Y. (2018). MTMR4, a phosphoinositide-specific 3'-phosphatase, regulates TFEB activity and the endocytic and autophagic pathways. Genes Cells.

Pietras, E.M., Reynaud, D., Kang, Y.-A., Carlin, D., Calero-Nieto, F.J., Leavitt, A.D., Stuart, J.M., Göttgens, B., and Passegué, E. (2015). Functionally Distinct Subsets of Lineage-Biased Multipotent Progenitors Control Blood Production in Normal and Regenerative Conditions. Cell Stem Cell *17*, 35–46.

Pu, J., Guardia, C.M., Keren-Kaplan, T., and Bonifacino, J.S. (2016). Mechanisms and functions of lysosome positioning. J. Cell Sci. *129*, 4329–4339.

Rapin, N., Bagger, F.O., Jendholm, J., Mora-Jensen, H., Krogh, A., Kohlmann, A., Thiede, C., Borregaard, N., Bullinger, L., Winther, O., et al. (2014). Comparing cancer vs normal gene expression profiles identifies new disease entities and common transcriptional programs in AML patients. Blood *123*, 894–904.

Recher, C. (2015). INPP4B, a new player in the chemoresistance of AML. Blood *125*, 2738–2739.

van Rhenen, A., Feller, N., Kelder, A., Westra, A.H., Rombouts, E., Zweegman, S., van der Pol, M.A., Waisfisz, Q., Ossenkoppele, G.J., and Schuurhuis, G.J. (2005). High stem cell frequency in acute myeloid leukemia at diagnosis predicts high minimal residual disease and poor survival. Clin. Cancer Res. *11*, 6520–6527.

Rijal, S., Fleming, S., Cummings, N., Rynkiewicz, N.K., Ooms, L.M., Nguyen, N.-Y.N., Teh, T.-C., Avery, S., McManus, J.F., Papenfuss, A.T., et al. (2015). Inositol polyphosphate 4-phosphatase II (INPP4B) is associated with chemoresistance and poor outcome in AML. Blood *125*, 2815–2824.

Saadatpour, A., Guo, G., Orkin, S.H., and Yuan, G.-C. (2014). Characterizing heterogeneity in leukemic cells using single-cell gene expression analysis. Genome Biol. *15*, 525.

Sardiello, M., Palmieri, M., di Ronza, A., Medina, D.L., Valenza, M., Gennarino, V.A., Di Malta, C., Donaudy, F., Embrione, V., Polishchuk, R.S., et al. (2009). A gene network regulating lysosomal biogenesis and function. Science *325*, 473–477.

Settembre, C., Zoncu, R., Medina, D.L., Vetrini, F., Erdin, S., Erdin, S., Huynh, T., Ferron, M., Karsenty, G., Vellard, M.C., et al. (2012). A lysosome-to-nucleus signalling mechanism senses and regulates the lysosome via mTOR and TFEB. EMBO J. *31*, 1095–1108.

Shlush, L.I., Mitchell, A., Heisler, L., Abelson, S., Ng, S.W.K., Trotman-Grant, A., Medeiros, J.J.F., Rao-Bhatia, A., Jaciw-Zurakowsky, I., Marke, R., et al. (2017). Tracing the origins of relapse in acute myeloid leukaemia to stem cells. Nature *547*, 104–108.

Somervaille, T.C.P., and Cleary, M.L. (2006). Identification and characterization of leukemia stem cells in murine MLL-AF9 acute myeloid leukemia. Cancer Cell *10*, 257–268.

Subramanian, A., Tamayo, P., Mootha, V.K., Mukherjee, S., Ebert, B.L., Gillette, M.A., Paulovich, A., Pomeroy, S.L., Golub, T.R., Lander, E.S., et al. (2005). Gene set enrichment analysis: a knowledge-based approach for interpreting genome-wide expression profiles. Proc Natl Acad Sci USA *102*, 15545–15550.

Valk, P.J.M., Verhaak, R.G.W., Beijen, M.A., Erpelinck, C.A.J., Barjesteh van Waalwijk van Doorn-Khosrovani, S., Boer, J.M., Beverloo, H.B., Moorhouse, M.J., van der Spek, P.J., Löwenberg, B., et al. (2004). Prognostically useful gene-expression profiles in acute myeloid leukemia. N. Engl. J. Med. *350*, 1617–1628.

Verhaak, R.G.W., Wouters, B.J., Erpelinck, C.A.J., Abbas, S., Beverloo, H.B., Lugthart, S., Löwenberg, B., Delwel, R., and Valk, P.J.M. (2009). Prediction of molecular subtypes in acute myeloid leukemia based on gene expression profiling. Haematologica *94*, 131–134.

Walter, R.B., Othus, M., Burnett, A.K., Löwenberg, B., Kantarjian, H.M., Ossenkoppele, G.J., Hills, R.K., Ravandi, F., Pabst, T., Evans, A., et al. (2015). Resistance prediction in AML: analysis of 4601 patients from MRC/NCRI, HOVON/SAKK, SWOG and MD Anderson Cancer Center. Leukemia *29*, 312–320.

Wang, P., Ma, D., Wang, J., Fang, Q., Gao, R., Wu, W., Cao, L., Hu, X., Zhao, J., and Li, Y. (2016). INPP4B-mediated DNA repair pathway confers resistance to chemotherapy in acute myeloid leukemia. Tumour Biol. *37*, 12513–12523.

Wouters, B.J., Löwenberg, B., Erpelinck-Verschueren, C.A.J., van Putten, W.L.J., Valk, P.J.M., and Delwel, R. (2009). Double CEBPA mutations, but not single CEBPA mutations, define a subgroup of acute myeloid leukemia with a distinctive gene expression profile that is uniquely associated with a favorable outcome. Blood *113*, 3088–3091.

Zhang, F., Zhu, J., Li, J., Zhu, F., and Zhang, P. (2017). IRF2-INPP4B axis participates in the development of acute myeloid leukemia by regulating cell growth and survival. Gene *627*, 9–14.

Zhang, F., Li, J., Zhu, J., Liu, L., Zhu, K., Cheng, S., Lv, R., and Zhang, P. (2019). IRF2-INPP4B-mediated autophagy suppresses apoptosis in acute myeloid leukemia cells. Biol. Res. *52*, 11.

Zuber, J., Radtke, I., Pardee, T.S., Zhao, Z., Rappaport, A.R., Luo, W., McCurrach, M.E., Yang, M.-M., Dolan, M.E., Kogan, S.C., et al. (2009). Mouse models of human AML accurately predict chemotherapy response. Genes Dev. *23*, 877–889.

Woolley *et al.* Figure 1

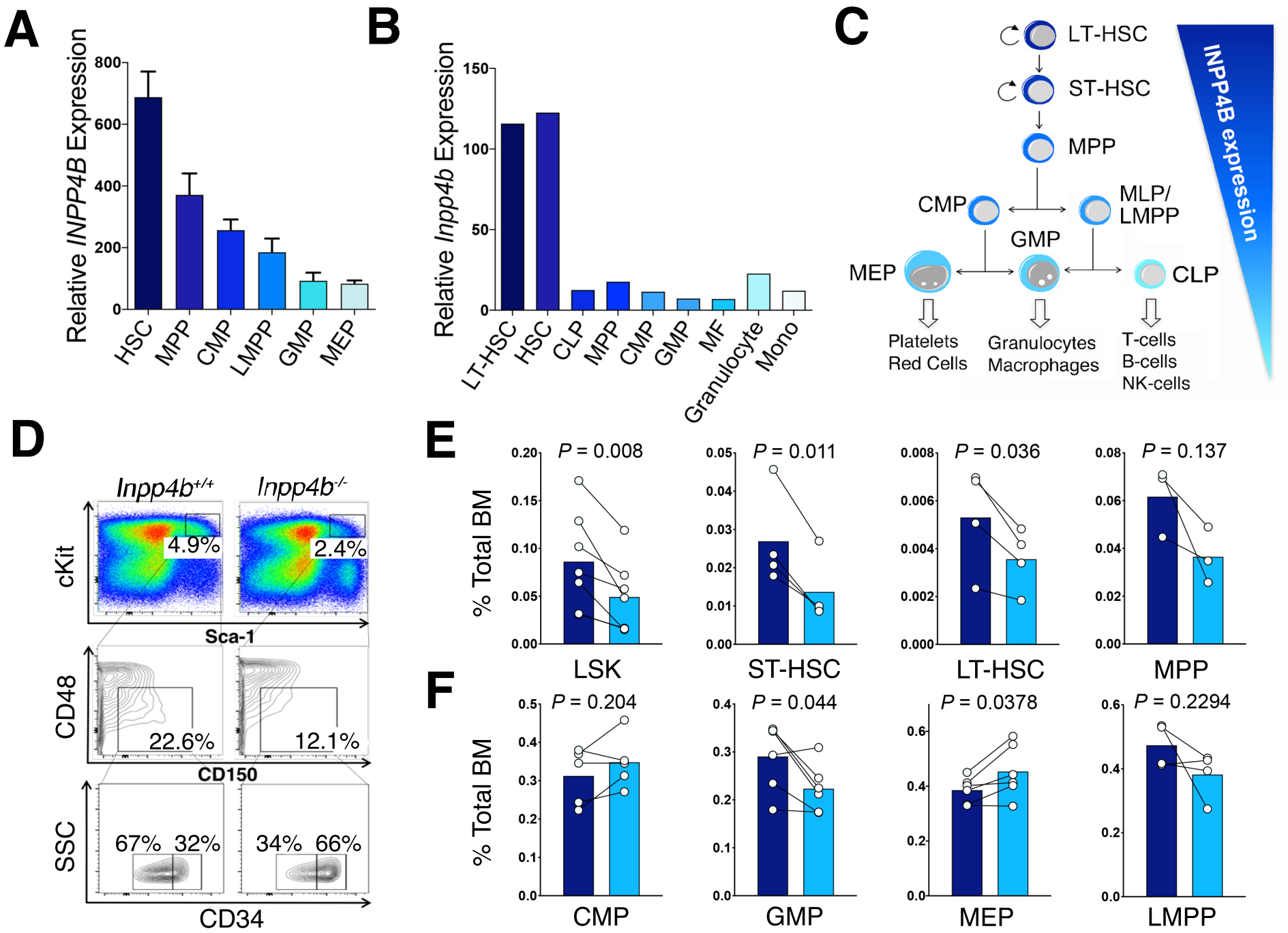

Woolley *et al.* Figure 2

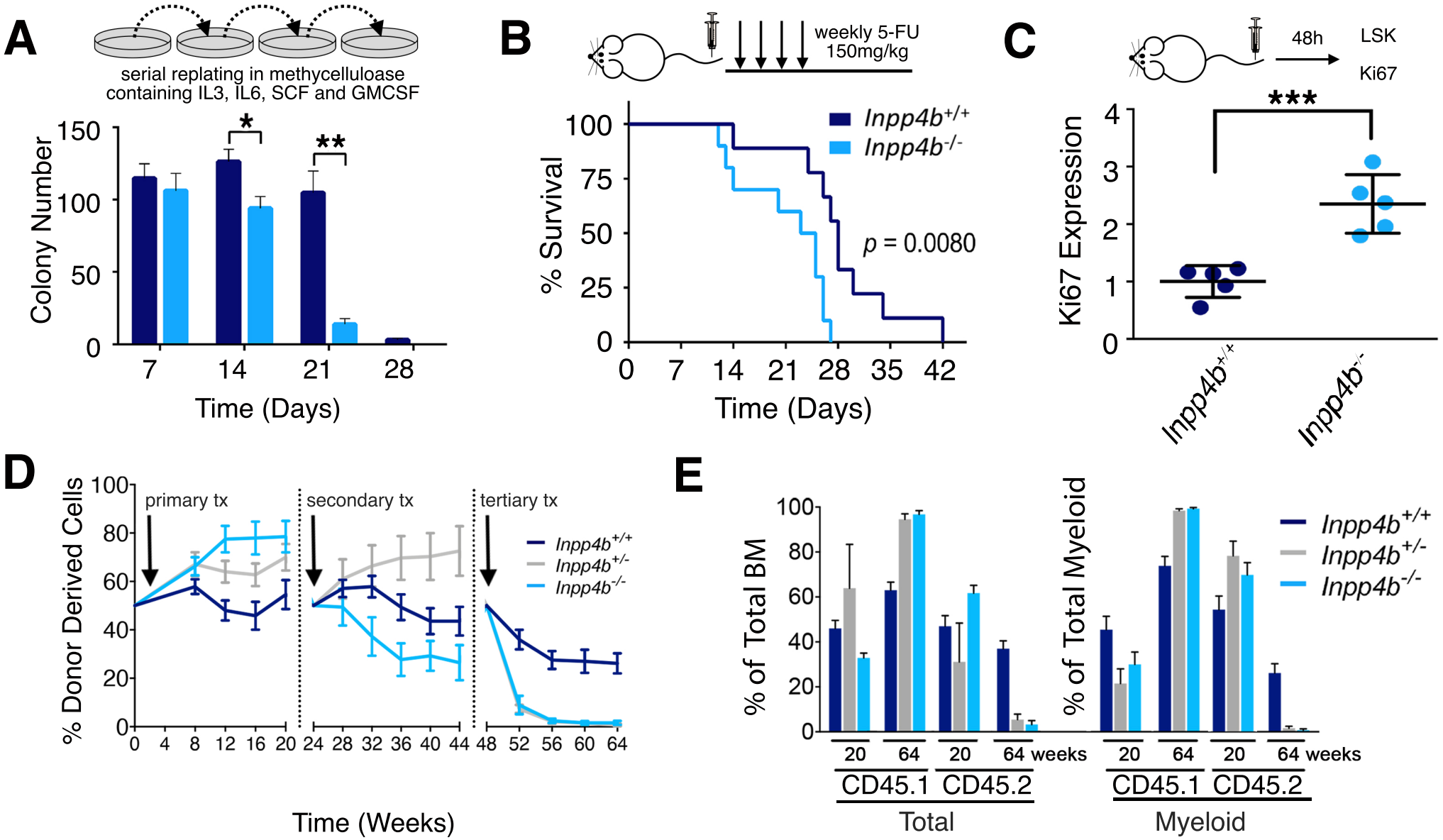

Woolley *et al.* Figure 3

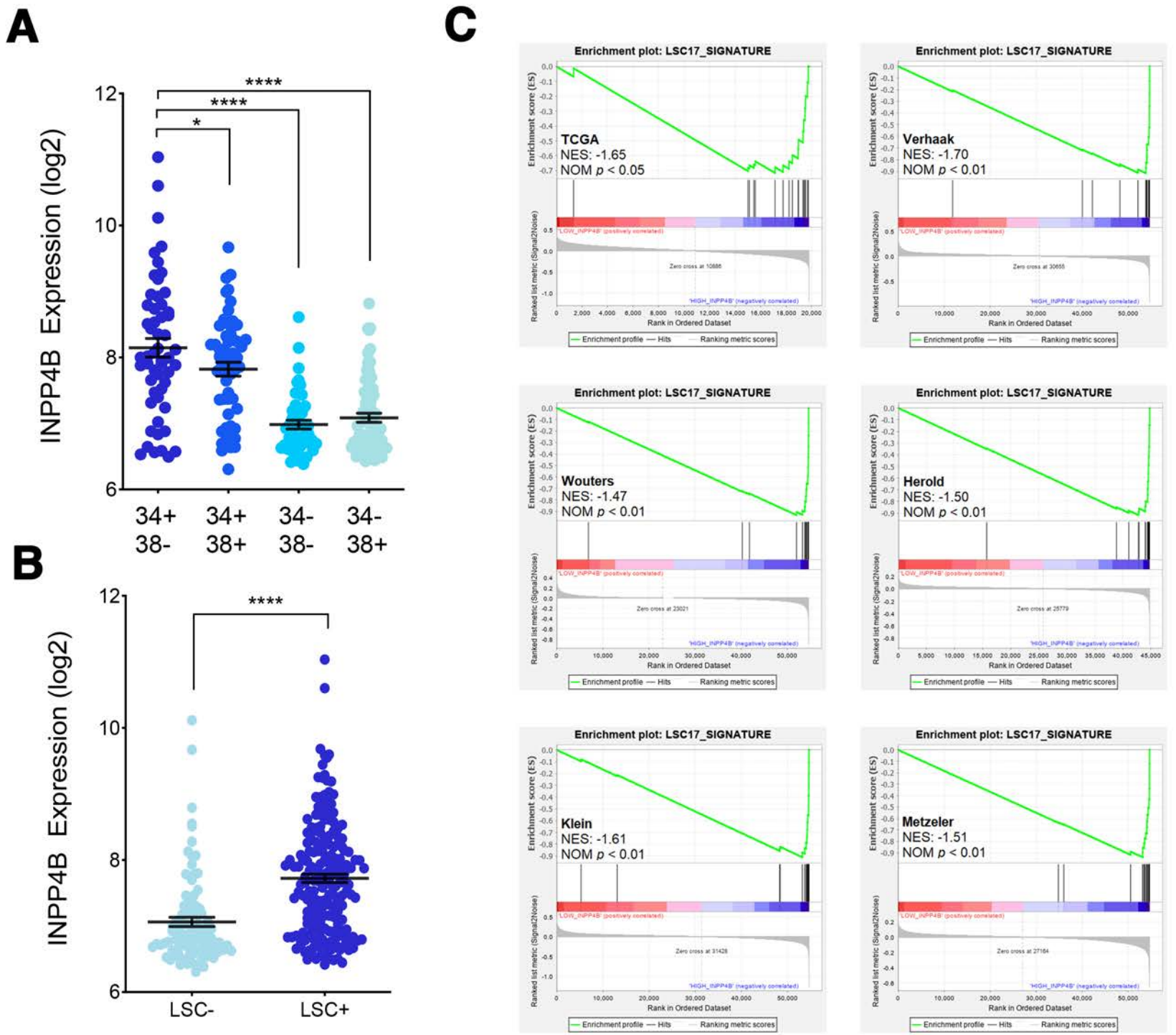

Woolley *et al.* Figure 4

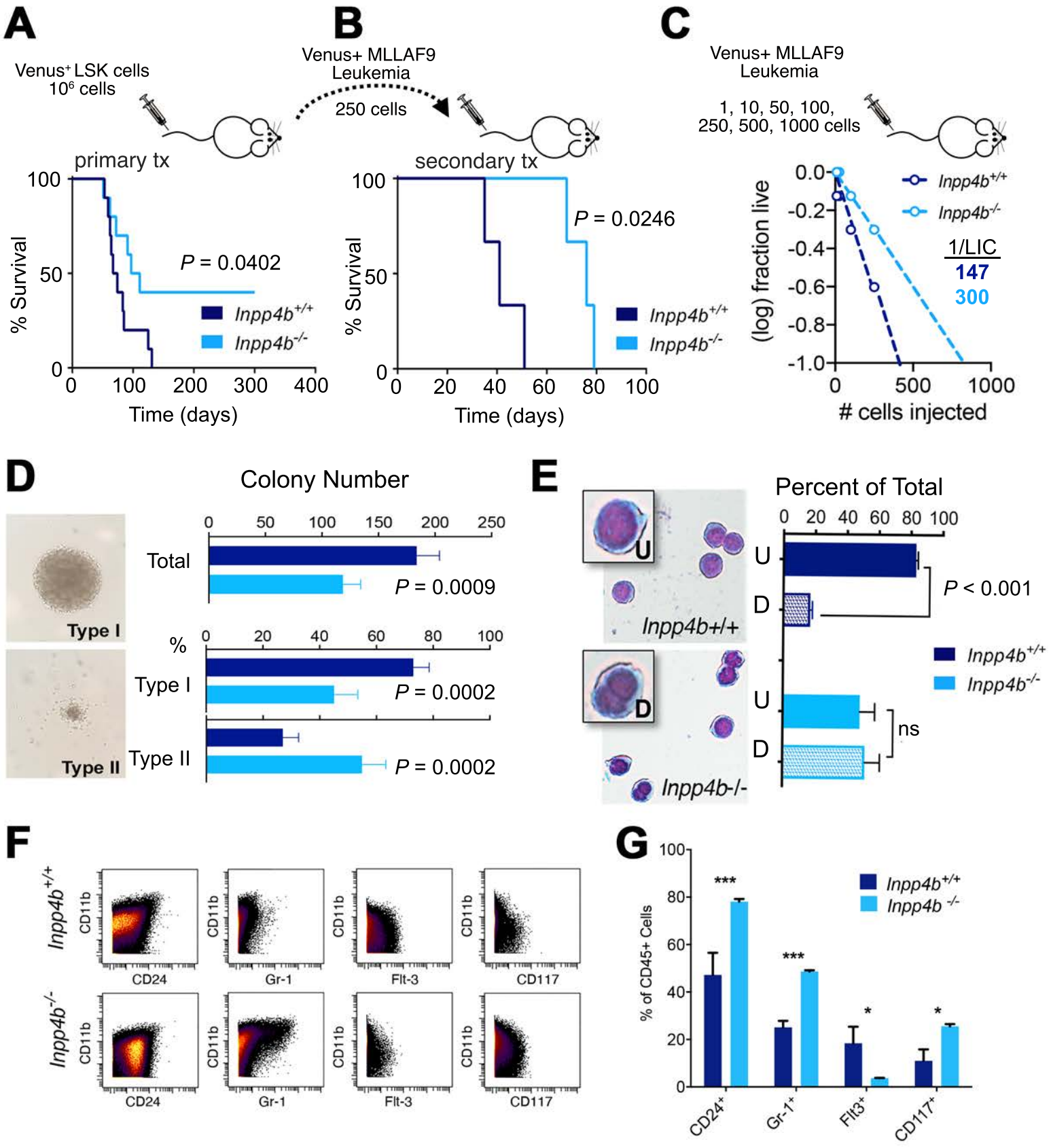

Woolley *et al.* Figure 5

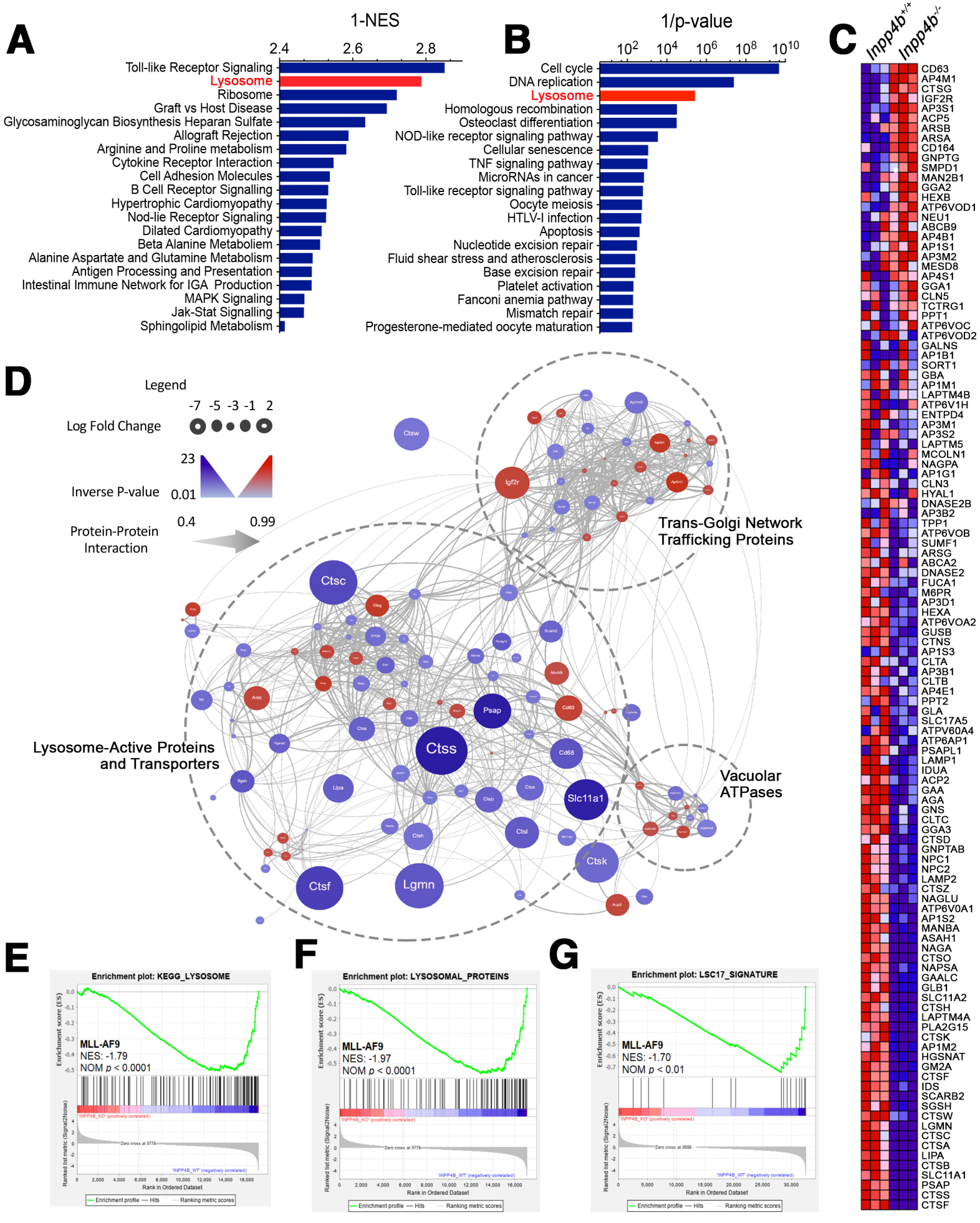

Woolley *et al*. Figure 6

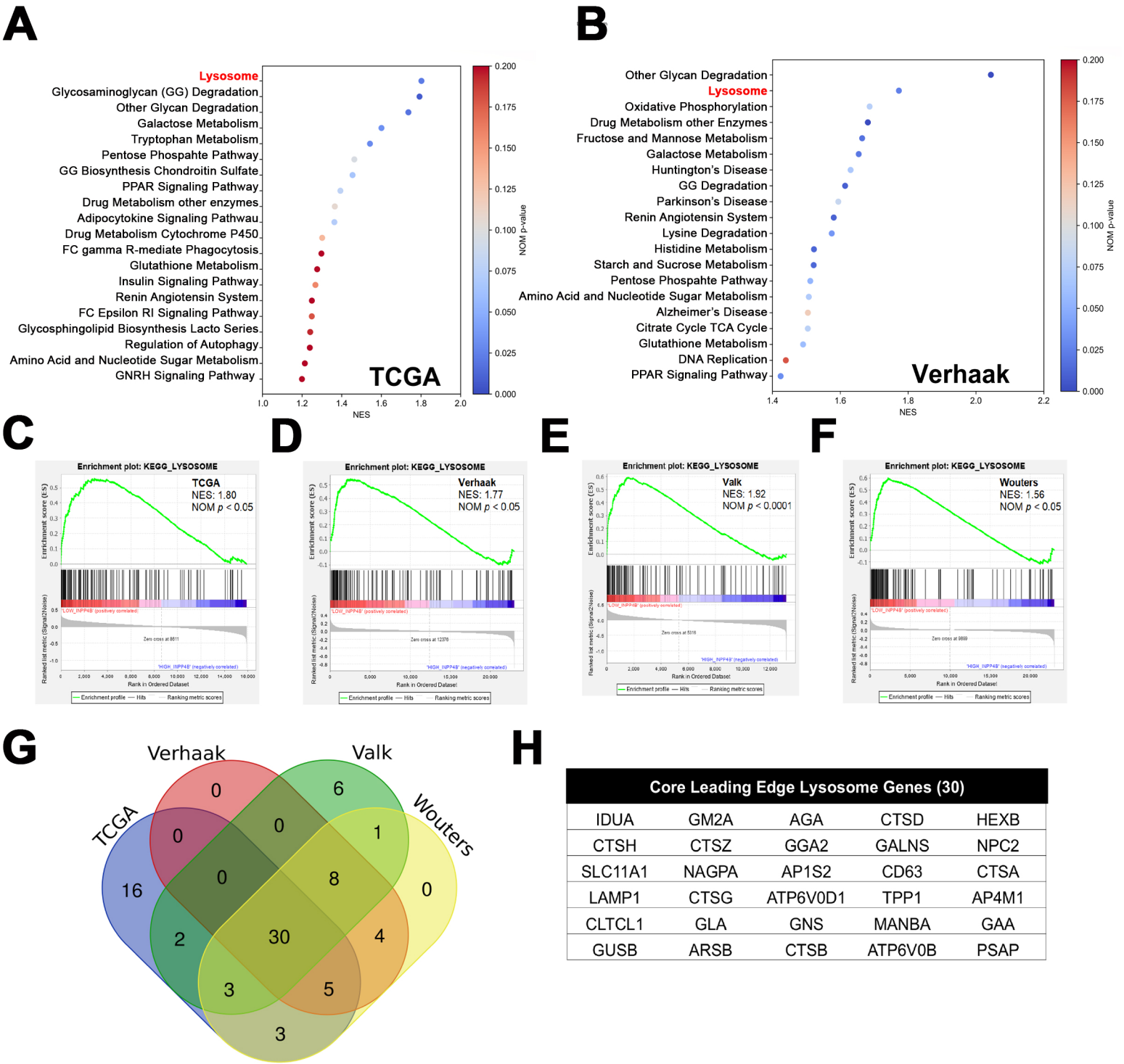

H

Core Leading Edge Lysosome Genes (30)				
IDUA	GM2A	AGA	CTSD	HEXB
CTSH	CTSZ	GGA2	GALNS	NPC2
SLC11A1	NAGPA	AP1S2	CD63	CTSA
LAMP1	CTSG	ATP6V0D1	TPP1	AP4M1
CLTCL1	GLA	GNS	MANBA	GAA
GUSB	ARSB	CTSB	ATP6V0B	PSAP

Woolley *et al*. Figure 7

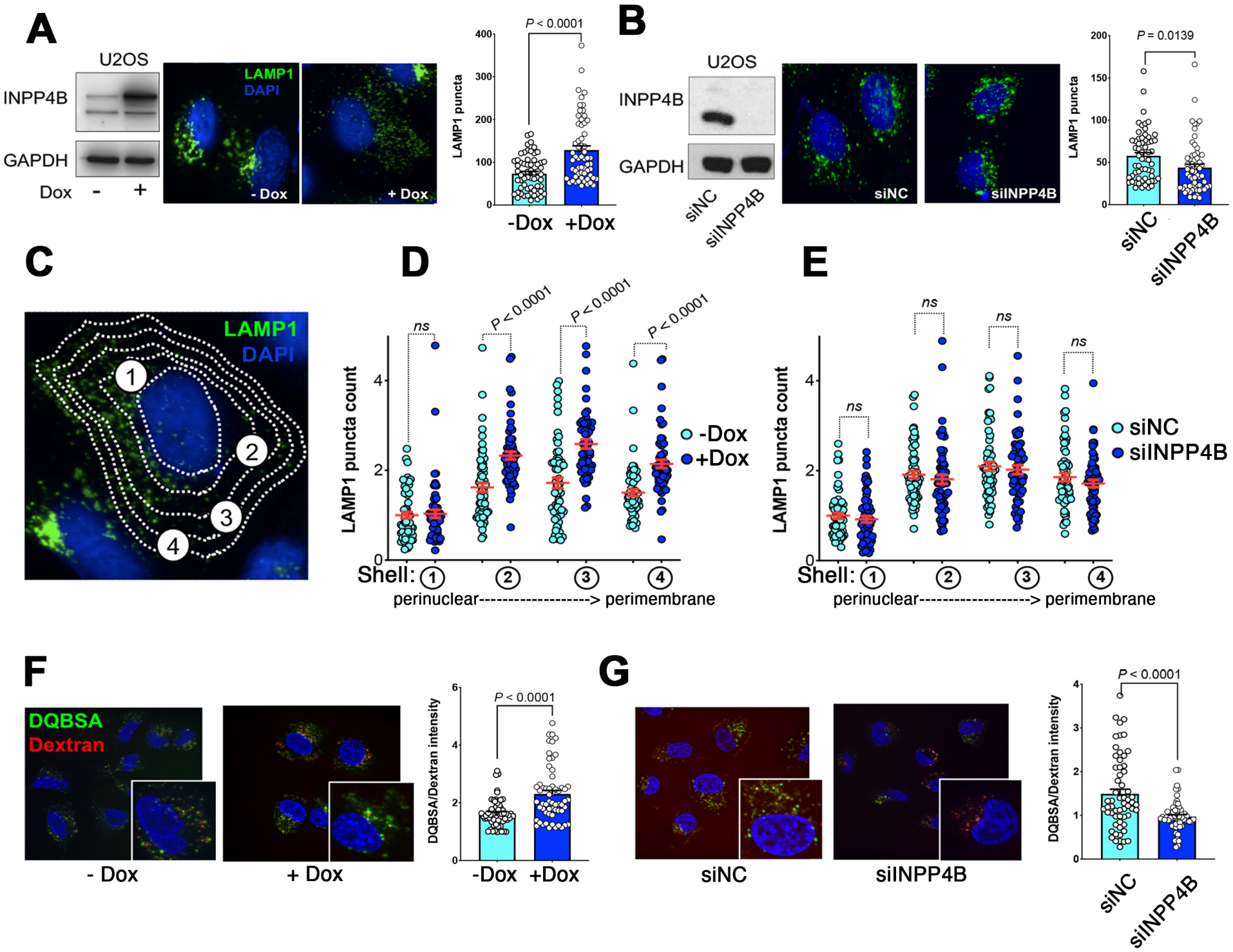

Woolley *et al*. Figure 8